Bioorganic & Medicinal Chemistry xxx (2016) xxx–xxx

Contents lists available at ScienceDirect

Bioorganic & Medicinal Chemistry

journal homepage: www.elsevier.com/locate/bmc

Synthesis and preclinical characterization of 1-(6′-deoxy-6′-[^{18}F]fluoro-β-D-allofuranosyl)-2-nitroimidazole (β-6′-[^{18}F]FAZAL) as a positron emission tomography radiotracer to assess tumor hypoxia

Thomas Wanek [a,*], Katharina Kreis [a], Petra Križková [b], Anna Schweifer [b,†], Christoph Denk [c], Johann Stanek [a], Severin Mairinger [a], Thomas Filip [a], Michael Sauberer [a], Patricia Edelhofer [a], Alexander Traxl [a], Viktoria E. Muchitsch [a], Kurt Mereiter [d], Friedrich Hammerschmidt [b], Carol E. Cass [e], Vijaya L. Damaraju [e], Oliver Langer [a,f], Claudia Kuntner [a]

[a] Biomedical Systems, AIT Austrian Institute of Technology GmbH, A-2444 Seibersdorf, Austria
[b] Institute of Organic Chemistry, University of Vienna, Währingerstraße 38, A-1090 Vienna, Austria
[c] Institute of Applied Synthetic Chemistry, Vienna University of Technology, Getreidemarkt 9/163, A-1060 Vienna, Austria
[d] Institute of Chemical Technologies and Analytics, Vienna University of Technology, Getreidemarkt 9/164, A-1060 Vienna, Austria
[e] Department of Oncology, University of Alberta, Edmonton, Alberta, Canada
[f] Department of Clinical Pharmacology, Medical University of Vienna, Währinger Gürtel 18-20, A-1090 Vienna, Austria

ARTICLE INFO

Article history:
Received 6 June 2016
Revised 16 August 2016
Accepted 27 August 2016
Available online xxxx

Keywords:
β-6′-[^{18}F]FAZAL
Pimonidazole
PET
Azomycin nucleosides

ABSTRACT

Positron emission tomography (PET) using fluorine-18 (^{18}F)-labeled 2-nitroimidazole radiotracers has proven useful for assessment of tumor oxygenation. However, the passive diffusion-driven cellular uptake of currently available radiotracers results in slow kinetics and low tumor-to-background ratios. With the aim to develop a compound that is actively transported into cells, 1-(6′-deoxy-6′-[^{18}F]fluoro-β-D-allofuranosyl)-2-nitroimidazole (β-[^{18}F]**1**), a putative nucleoside transporter substrate, was synthetized by nucleophilic [^{18}F]fluoride substitution of an acetyl protected labeling precursor with a tosylate leaving group (β-**6**) in a final radiochemical yield of 12 ± 8% (n = 10, based on [^{18}F]fluoride starting activity) in a total synthesis time of 60 min with a specific activity at end of synthesis of 218 ± 58 GBq/μmol (n = 10). Both radiolabeling precursor β-**6** and unlabeled reference compound β-**1** were prepared in multistep syntheses starting from 1,2:5,6-di-*O*-isopropylidene-α-D-allofuranose. In vitro experiments demonstrated an interaction of β-**1** with SLC29A1 and SLC28A1/2/3 nucleoside transporter as well as hypoxia specific retention of β-[^{18}F]**1** in tumor cell lines. In biodistribution studies in healthy mice β-[^{18}F]**1** showed homogenous tissue distribution and excellent metabolic stability, which was unaffected by tissue oxygenation. PET studies in tumor bearing mice showed tumor-to-muscle ratios of 2.13 ± 0.22 (n = 4) at 2 h after administration of β-[^{18}F]**1**. In ex vivo autoradiography experiments β-[^{18}F]**1** distribution closely matched staining with the hypoxia marker pimonidazole. In conclusion, β-[^{18}F]**1** shows potential as PET hypoxia radiotracer which merits further investigation.

1. Introduction

A variety of solid tumors exhibit oxygen deficiency as a result of their rapid growth and/or insufficient tumor angiogenesis.[1] Due to this shortage in blood supply, the distribution of oxygen within a tumor diminishes towards the less vascularized center of the tumor, ultimately resulting in hypoxia.[2,3] Tumor hypoxia is associated with an aggressive phenotype, poor prognosis, increased risk of invasion and metastasis, and finally resistance to chemo- and radiation therapy.[4] Positron emission tomography (PET) utilizing fluorine-18 labeled 2-nitroimidazole radiotracers has been shown to be a suitable imaging technique due to its non-invasive nature and the possibility to accurately quantify hypoxic regions within tissues. These radiotracers pass the cell membrane through passive diffusion and are reduced intracellularly in all viable cells to free nitro-radical anions which are further reduced to nitroso- and

Abbreviations: SUV, standardized uptake value; SD, standard deviation; SE, standard error; TLC, thin-layer chromatography; iv, intravenous.

* Corresponding author. Tel.: +43 50 550 3496; fax: +43 50 550 2136.
E-mail address: thomas.wanek@ait.ac.at (T. Wanek).
† Deceased.

http://dx.doi.org/10.1016/j.bmc.2016.08.053
0968-0896/

hydroxylamine compounds if hypoxic conditions are present.[5–7] The binding of the such formed hydroxylamine compounds to macromolecules as well as the formation of glutathione conjugates has been recently shown to be the major contributor to radiotracer accumulation in hypoxic regions of tumors.[8]

Fluorine-18 labeled misonidazole ([^{18}F]FMISO, Fig. 1) was one of the first PET radiotracers used clinically showing a wide applicability for many cancer types.[9–13] However, [^{18}F]FMISO accumulates slowly in hypoxic (target) tissue and the slow washout of unbound (hypoxia unrelated) tracer results in modest hypoxic-to-normoxic tissue ratios and therefore images with moderate contrast. Moreover, its predominately hepatic clearance results in a high radiation dose delivered to the liver and the presence of radiolabeled metabolites in blood and urine further limits its utility.[14] To overcome these limitations, efforts mainly focused on synthesizing compounds exhibiting a careful balance between sufficiently high diffusion into target cells and rapid clearance from non-target cells.[6,15] In particular 2-nitroimidazole compounds containing sugar-moieties showed great promise such as the nucleoside analogue 1-(5′-deoxy-5′-[^{18}F]fluoro-α-D-arabinofuranosyl)-2-nitroimidazole (α-5′-[^{18}F]FAZA, Fig. 1), which displays a hypoxia-specific uptake with tumor-to-background ratios superior to [^{18}F]FMISO due to its faster clearance from blood.[16–20]

However, efforts to improve the imaging characteristics of hypoxia radiotracers are limited by the passive diffusion-driven cellular uptake. It has been suggested, that the exploitation of naturally occurring transmembrane transporter systems, such as glucose transporters (e.g., SLC2A family) or nucleoside transporters (e.g., SLC28A and SLC29A families), may lead to a faster entry of the radiotracer into viable cells. In particular bidirectional transporters like SLC29A1 would provide excellent targets for this concept, as they facilitate transfer of their substrates into both directions, either into the cell, which would increase radiotracer entry into cells, or out of the cell, which would increase clearance of non-bound radiotracer from non-target tissues. Consequently, when retained under hypoxic conditions, this may result in an improved imaging contrast especially at earlier time frames. These considerations have led to the development of 1-(2′-deoxy-2′-[^{18}F]fluoro-β-D-glucopyranosyl)-2-nitroimidazole (β-2′-[^{18}F]FDG-2-NIm, Fig. 1) which was shown to be transported by glucose transporters but failed to show retention in hypoxic tissue.[21] To utilize nucleoside transporters, β-analogues of α-5′-[^{18}F]FAZA have been synthetized, such as 1-(5′-deoxy-5′-[^{18}F]fluoro-β-D-ribofuranosyl)-2-nitroimidazole (β-5′-[^{18}F]FAZR), 1-(2′-deoxy-2′-[^{18}F]fluoro- β-D-arabinofuranosyl)-2-nitroimidazole (β-2′-[^{18}F]FAZA) and 1-(3′-deoxy-3′-[^{18}F]fluoro-β-D-xylofuranosyl)-2-nitroimidazole (β-3′-[^{18}F]FAZL, Fig. 1).[22,23] However, these radiotracers have not yet been characterized with respect to their ability to image tumor hypoxia in vivo.

The C(3′)-OH, C(2′)-OH and C(5′)-OH of the sugar moiety were shown to be structural determinants of nucleoside interaction with SLC29A1/2 and SLC28A1/2/3 transporters.[24] With the aim to leave these positions unchanged for such a transporter interaction we designed 1-(6′-deoxy-6′-[^{18}F]fluoro-β-D-allofuranosyl)-2-nitroimidazole (β-6′-[^{18}F]FAZAL; β-[^{18}F]**1**, Fig. 1) and herein report the precursor synthesis, radiosynthesis and preclinical evaluation as a potential hypoxia radiotracer.

2. Results and discussion

2.1. Chemistry and radiolabeling

The synthesis of 1-(2′,3′,5′-tri-*O*-acetyl-6-*O*-*p*-toluenesulfonyl-β-D-allofuranosyl)-2-nitroimidazole (β-**6**), the radiolabeling precursor of β-[^{18}F]**1**, is shown in Scheme 1. First, commercially available 1,2:5,6-di-*O*-isopropylidene-α-D-allofuranose was converted into known 5,6-diol **2** in 85% yield by acetylation and removal of the 5,6-*O*-isopropylidene group, using literature procedures.[25] Derivative **2** was selectively monotosylated at the C-6 hydroxyl group with *p*-toluenesulfonyl chloride in pyridine to give compound **3** in 74% yield. The reaction was carried out at −25 °C to prevent the formation of the 5,6-ditosylate, which was significant at +4 °C. Compound **3** was acetylated with acetic anhydride (Ac_2O)/pyridine to afford **4**. Removal of the 1,2-isopropylidene group in **4** with 60% aqueous TFA followed by acetylation with Ac_2O in pyridine provided a 3:1 mixture of α- and β-allofuranose tetraacetates α- and β-**5** in 78% combined yield for the two steps. The coupling of these tetraacetates with 2-nitroimidazole was the critical step of the sequence. It was accomplished by a modified Vorbrüggen protocol.[26] Commercially available 2-nitroimidazole was first triethylsilylated with hexaethyldisilazane in pyridine and then reacted with the mixture of tetraacetates in CH_3CN, catalyzed by triethylsilyl triflate. The ratio of the formed nucleosides was dependent on the reaction temperature. At 0 °C and a reaction time of 1 h, the β-nucleoside β-**6** was obtained in 44% and the α-nucleoside in 5% yield. At rt the two anomers were formed in a combined yield of 45% in an $\alpha:\beta$ ratio of 20:25. The configuration at the anomeric centers was assigned on the basis of the coupling constants between 1-H and 2-H (α-anomer: $J_{1,2}$ = 5.3 Hz; β-anomer: $J_{1,2}$ = 4.2 Hz) in the ^{1}H NMR spectrum. It is noteworthy that the 2-nitroimidazole nucleoside β-**6** crystallized as a solvate with 0.5 mol of $CHCl_3$ from $CHCl_3$/EtOAc or with 0.5 mol of EtOAc from EtOAc/iPr$_2$O.

The unlabeled reference standard β-**1** was also prepared from 1,2:5,6-di-*O*-isopropylidene α-D-allofuranose (Scheme 2). It was converted into the α-D-allofuranose triol 7 in 77% yield, using 60% aqueous AcOH. Mitsunobu reaction in toluene with triphenylphosphane/diisopropyl azodicarboxylate (DIAD) gave exclusively epoxide **8** in 89% yield without changing the configuration at C-5.[27] The oxirane ring was selectively opened by fluoride at C-6 using TBABF/KHF_2 in toluene, followed by diacetylation of the intermediate 3,5-diol to give 6-fluoro derivative **9** in an overall yield of 86%.[28] The 1,2-isopropylidene group in **9** was removed with 60% aqueous TFA and the free hydroxyl groups at C-1 and C-2 were acetylated to give the anomeric fluoro tetraacetates **10** ($\alpha:\beta$ = 3:1 by ^{1}H NMR) in 70% yield. In analogy to the synthesis of radiolabeling precursor (Scheme 1), the mixture of α- and β-10 was coupled with triethylsilylated 2-nitroimidazole to yield an α, β-mixture of tetraacetates **11**. After a reaction time of 15 min at 0 °C the $\alpha:\beta$ ratio in the crude product was 1.0:3.9 as determined by ^{1}H NMR spectroscopy and isolated yields after flash chromatography were 8% and 44%, respectively. The diagnostic coupling constants $J_{1,2}$ of the anomers (α-**11**: $J_{1,2}$ = 5.3 Hz; β-**11**: $J_{1,2}$ = 4.4 Hz) were very similar to the ones of the radiolabeling precursors α- and β-**6**. The assignment of the configuration of crystalline α-**11**, but not of foamy β-**11**, and consequently also of the other anomers of **6** and **11**, was secured by single crystal X-ray structure analysis (for details see Supporting information). Zemplen saponification of β-**11** provided the unlabeled reference standard 1-(6′deoxy-6′-fluoro-β-D-allofuranosyl)-2-nitroimidazole nucleoside (β-**1**), in 61% yield.

Radiosynthesis of β-[^{18}F]**1** was performed by nucleophilic substitution of the tosylate leaving group in precursor β-**6** with [^{18}F] fluoride followed by hydrolysis of the acetyl protective groups (Scheme 3). We initially performed manual radiolabeling experiments in order to identify suitable reaction parameters for the automated radiosynthesis. Initially, kryptofix 2.2.2 and K_2CO_3 were used in the nucleophilic substitution reaction, which did not form the desired product irrespective of labeling temperature, reaction time and solvent. When tetrabutylammonium hydrogen carbonate was used, the desired product (acetylated β-[^{18}F]**1**) was formed.

Please cite this article in press as: Wanek, T.; et al. *Bioorg. Med. Chem.* (2016), http://dx.doi.org/10.1016/j.bmc.2016.08.053

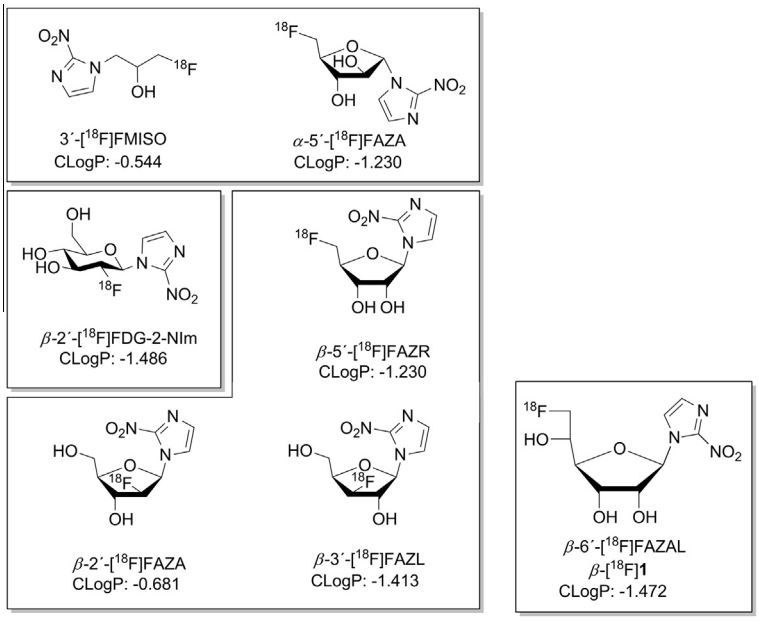

Figure 1. Chemical structures and calculated lipophilicity of the established fluorine-18 labeled hypoxia radiotracers [^{18}F]FMISO and α-5′-[^{18}F]FAZA, the sugar-coupled 2-nitroimidazole derivatives susceptible to active transport by glucose transporters (β-2′-[^{18}F]FDG-2-NIm) or nucleoside transporters (β-5′-[^{18}F]FAZR, β-2′-[^{18}F]FAZA and β-3′-[^{18}F]FAZL) as well as the reported compound β-6′-[^{18}F]FAZAL (β-[^{18}F]**1**). CLogP values were calculated using ChemDraw v15 software.

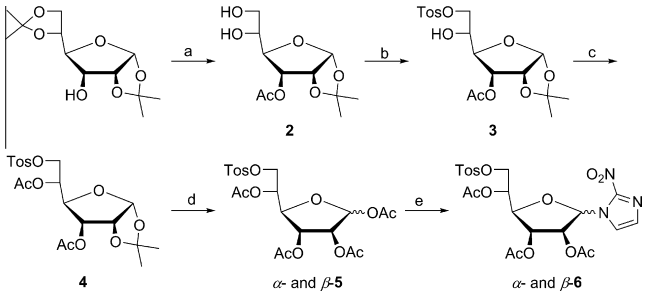

Scheme 1. Synthesis of radiolabeling precursor β-**6**. Reagents and conditions: (a) (i) Ac_2O, py, (ii) 60% AcOH, 85%; (b) *p*-TosCl, py, CH_2Cl_2, 74%; (c) Ac_2O, py, CH_2Cl_2, quant. yield; (d) (i) 60% TFA, (ii) Ac_2O, py, CH_2Cl_2, 78%, α/β = 3:1; (e) (i) 2-nitroimidazole, hexaethyldisilazane, py, (ii) $TfOSiEt_3$, CH_3CN, 49%, α/β = 1:9.

Our failure to obtain product with kryptofix 2.2.2/K_2CO_3 points to a base sensitivity of the labeling precursor β-**6**, which could be overcome by the use of less basic tetrabutylammonium hydrogen carbonate. Labeling yield depended on the reaction temperature and increased for a reaction time of 10 min using 5 mg precursor from 4% at 75 °C to 44% at 120 °C. A slow degradation of the radiolabeling precursor β-**6** was observed at a temperature >120 °C. The automated synthesis of β-[^{18}F]**1** was performed by reacting 7 mg of precursor β-**6** with dried tetrabutylammonium [^{18}F]fluoride complex dissolved in anhydrous DMSO for 8 min at 115 °C and subsequent deprotection with 0.25 M aqueous sodium hydroxide solution. β-[^{18}F]**1**, ready for intravenous injection, was obtained in a decay-corrected radiochemical yield of 12 ± 8% (n = 10, based on [^{18}F]fluoride starting activity) in a total synthesis time of 60 min. Further efforts to improve the radiochemical yield of the automated synthesis procedure are currently in progress. Radiochemical purity was greater than 96% (see Supporting information for representative radio-HPLC and TLC chromatograms) and the specific activity at the end of synthesis was 218 ± 58 GBq/μmol (n = 10). Final formulated β-[^{18}F]**1** solution had a pH of 5.4 ± 0.3 and an osmolarity of 320 ± 73 mosmol/kg.

2.2. Inhibition of [^{3}H]uridine transport by unlabeled β-1

Interaction of β-**1** with nucleoside transporters SLC29A1/2 and SLC28A1-3 was confirmed by determining the capability of β-**1** to inhibit [^{3}H]uridine uptake in yeast cells expressing recombinant human nucleoside transporters. Half-maximum inhibitory

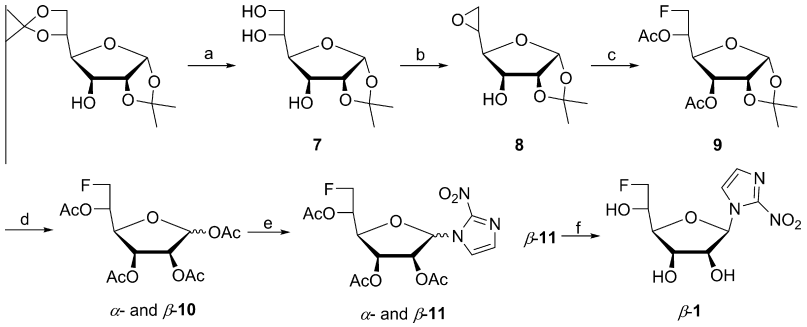

Scheme 2. Synthesis of reference standard β-**1**. Reagents and conditions: (a) 60% AcOH, 77%; (b) Ph_3P, DIAD, toluene, 89%; (c) (i) TBABF, KHF_2, toluene, (ii) Ac_2O, py, 86%; (d) (i) 60% TFA, (ii) Ac_2O, py, CH_2Cl_2, 70%, α/β = 3:1; (e) (i) 2-nitroimidazole, hexaethyldisilazane, py, (ii) $TfOSiEt_3$, CH_3CN, 52%, α/β = 1:6; (f) CH_3ONa, CH_3OH, 61%.

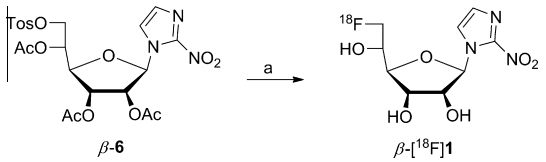

β-**6** β-[^{18}F]**1**

Scheme 3. Radiosynthesis of β-[^{18}F]**1**. Reagents and conditions: (a) (i) [^{18}F]HF, $[(Bu)_4N]^+HCO_3^-$, DMSO (ii) NaOH.

concentrations (IC_{50}) were determined and compared to those for thymidine measured with the same transport assay in the same laboratory as published previously (Table 1).[22] The observed IC_{50} values confirmed an interaction of β-**1** with SLC29A1 and SLC28A1/2/3 nucleoside transporters with the rank order: SLC28A1 > SLC28A3 > SLC29A1. No interaction of β-**1** with SLC29A2 was observed. IC_{50} values were higher than those of thymidine suggesting lower transmembrane transporter affinities.

Table 1
Inhibition of [^{3}H]uridine transport by β-**1** in yeast cells stably transfected with cDNAs encoding human nucleoside transporters. Data are expressed as mean ± SE for n = 2–3 experiments

Nucleoside transporter	IC_{50} (μM)	
	Thymidine[a]	β-**1**
SLC29A1 (hENT1)	76 ± 18	840 ± 22
SLC29A2 (hENT2)	160 ± 10	NI
SLC28A1 (hCNT1)	22 ± 3	630 ± 343
SLC28A2 (hCNT2)	1200 ± 210	>1000
SLC28A3 (hCNT3)	35 ± 5	770 ± 74

NI—no interaction.
[a] Data taken from Ref 21, measured in same laboratory.

2.3. Cell uptake studies of β-[^{18}F]1

In vitro uptake of β-[^{18}F]**1** was assessed in murine mammary carcinoma cells EMT6 and human non-small cell lung cancer cells NCI-H1975 incubated either in hypoxic (1% O_2) or normoxic (21% O_2) atmosphere. Cell viability was assessed by WST-1 (4-[3-(4-iodophenyl)-2-(4-nitrophenyl)-2*H*-5-tetrazolio]-1,3-benzene-disulfonate) viability assay, which confirmed that both cell lines maintained >80% viability when cultured under hypoxic conditions compared to normoxic conditions (see Supporting information). As a further control experiment, glycolytic activity in EMT6 and NCI-H1975 cells was compared using [^{18}F]FDG, for which uptake increased steadily in both cell lines during the observation period. Interestingly, [^{18}F]FDG uptake was significantly higher in hypoxic compared to normoxic EMT6 cells at 3 and 5 h after start of incubation. In contrast, in NCI-H1975 cells, [^{18}F]FDG uptake over time was not different between hypoxic or normoxic incubated cells. This observation could be related to different response times in the recruitment of glucose transporters to the cell membrane, or differences in hexokinase activity between human and murine cells (see Supporting information).[29]

In both cell lines, uptake of β-[^{18}F]**1** increased steadily when cells were incubated under hypoxic conditions whereas uptake remained relatively stable under normoxic atmosphere (Fig. 2A and B). Moreover, the lack of accumulation in normoxic cells, especially in NCI-H1975 cells which express high levels of SLC29A1, suggests that cellular retention of β-[^{18}F]**1** does not depend on SLC29A1 expression levels.[30] The hypoxic-to-normoxic ratio in EMT6 cells increased from 0.85 ± 0.13 at 1 h to 4.68 ± 0.61 at 3 h and 4.98 ± 0.83 at 5 h. In NCI-H1975 cells, total radioactivity uptake was lower when compared to EMT6 cells. Hypoxic-to-normoxic ratios in NCI-H1975 cells increased from 0.9 ± 0.13 at 1 h to 1.87 ± 0.34 at 3 h and 3.73 ± 0.41 at 5 h incubation time. The observed increase in hypoxic-to-normoxic ratio over time observed in both cell lines suggest a hypoxia sensitive retention of β-[^{18}F]**1** and is in line with observations reported for other, confirmed hypoxia sensitive compounds. For example, in a comparable experiment, the hypoxic-to-normoxic uptake ratio for α-5′-[^{18}F]FAZA increased from 1.4 at 20 min to 2.7 at 100 min in Walker 256 rat tumor cells. Similarly, [^{18}F]FMISO uptake ratio increased from 1.5 at 20 min to 3.0 at 100 min in the same study.[19] Furthermore, for a number of other compounds developed for hypoxia imaging increased cellular uptake has been observed under hypoxic conditions.[31,32] Additionally, the effect of inhibition of nucleoside transporter activity on β-[^{18}F]**1** uptake was examined in EMT6 and NCI-H1975 cells under normoxic and hypoxic conditions. For this, the accumulation of β-[^{18}F]**1** after 10 min incubation time in the absence (buffer) or presence of 10 μM dipyridamole or nitrobenzylmercaptopurine ribonucleoside (NBMPR), two established SLC29A1 inhibitors, was determined.[24,30] Both nucleoside transporter inhibitors significantly reduced β-[^{18}F]**1** uptake in normoxic and hypoxic tumor cells, suggesting that SLC29A1 activity determines early cell accumulation of β-[^{18}F]**1** irrespective of the atmospheric conditions (Fig. 2C and D).

2.4. Biodistribution and metabolism in nude mice

Biodistribution and metabolism of β-[^{18}F]**1** were assessed in isoflurane anesthetized female NMRI-Foxn1^{nu} mice at 2 h after intravenous injection. To assess the influence of tissue oxygenation on tissue pharmacokinetics and formation of radiolabeled metabolites, we studied two groups of mice with different breathing protocols. In one group isoflurane was delivered to the animals in pure oxygen (100% O_2) and in the other group in medical air (21% O_2). It has been shown previously that this procedure significantly affects oxygen levels in various tissues and tumors and can be utilized for preclinical evaluation of hypoxia sensitive compounds.[33,34] Two hours after injection, β-[^{18}F]**1** displayed homogeneous distribution in all investigated tissues and the radioactivity concentration in most tissues was comparable to that in blood (Table 2).

Very high radioactivity concentrations were measured in urine suggesting renal excretion as major clearance route of β-[^{18}F]**1**. Bone radioactivity concentration was comparably low, pointing to a low degree of in vivo de-fluorination. Uptake of β-[^{18}F]**1** in liver tissue was considerably lower than values reported for [^{18}F]FMISO, and in the same range as for α-5′-[^{18}F]FAZA at 3 h post injection.[35] The different breathing protocols afforded no significant differences in the biodistribution of β-[^{18}F]**1** (2-way ANOVA). Only a low percentage (<10%) of radiolabeled metabolites was detected in plasma and urine at 2 h post injection (Table 3).

Metabolic stability of β-[^{18}F]**1** appeared to be better than for [^{18}F]FMISO (50% and 64% unchanged parent in mouse plasma and urine at 2 h after injection, respectively) and α-5′-[^{18}F]FAZA (73% unchanged parent in urine at 1 h post injection).[14,35] The low amount of circulating radiolabeled metabolites may lead to improved tumor-to-background ratios for β-[^{18}F]**1** as compared with extensively metabolized hypoxia tracers. Formation of radiolabeled metabolites appeared to be independent of employed breathing protocol, which is desirable as an oxygen dependent metabolism may confound the interpretation of PET data.

2.5. PET study in a murine hypoxia tumor model

EMT6 cells were chosen as hypoxia tumor model as this model was shown to contain a relatively large (40%) fraction of hypoxic areas when grown in vivo.[36,37] PET and magnetic resonance

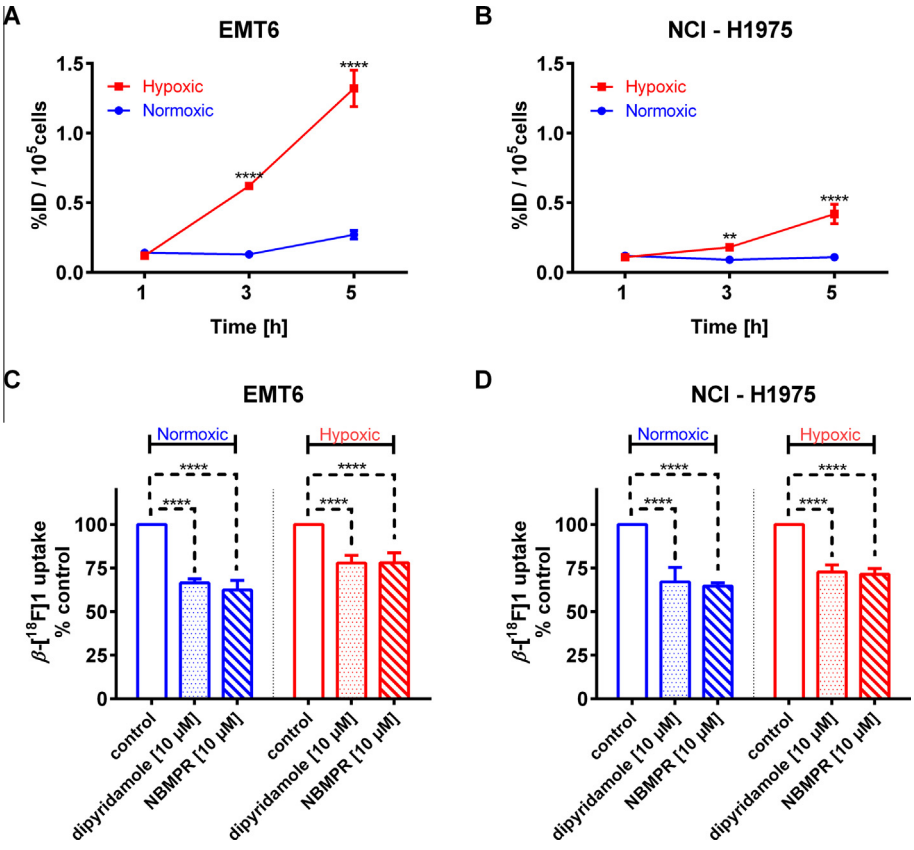

Figure 2. In vitro cell uptake of β-[^{18}F]**1** in (A) EMT6 and (B) NCI-H1975 cells incubated under normoxic (21% O_2) and hypoxic (1% O_2) conditions. Data are presented as decay corrected mean percent incubated dose (ID) ± standard deviation (SD) and differences compared between normoxic and hypoxic conditions. Uptake of β-[^{18}F]**1** in (C) EMT6 and (D) NCI-H1975 cells after 10 min incubation time in absence or presence of the nucleoside transporter inhibitors dipyridamole and nitrobenzylmercaptopurine ribonucleoside (NBMPR). Values are shown as percentage of control values obtained in absence of the respective inhibitor. $^{**}p$ <0.01; $^{****}p$ <0.0001 (2-way ANOVA).

Table 2
Biodistribution of β-[^{18}F]**1** at 120 min after injection into NMRI-*Foxn1^{nu}* mice breathing either isoflurane/oxygen or isoflurane/air

Tissue	Isoflurane/oxygen	Isoflurane/air
Blood	0.14 ± 0.02	0.11 ± 0.01
Plasma	0.14 ± 0.03	0.11 ± 0.02
Lung	0.13 ± 0.03	0.12 ± 0.02
Spleen	0.26 ± 0.17	0.18 ± 0.06
Liver	0.18 ± 0.04	0.16 ± 0.04
Kidneys	0.35 ± 0.07	0.31 ± 0.07
Urine	33.63 ± 28.53	14.93 ± 2.11
Heart	0.17 ± 0.02	0.13 ± 0.05
Small intestine	0.21 ± 0.04	0.23 ± 0.06
Large intestine	0.18 ± 0.02	0.23 ± 0.02
Brain	0.03 ± 0.00	0.03 ± 0.00
Muscle	0.13 ± 0.02	0.14 ± 0.04
Bone	0.11 ± 0.01	0.09 ± 0.02

Data are expressed as mean SUV ± SD (n = 4–6).

Table 3
Percent unchanged β-[^{18}F]**1** (mean ± SD, n = 4–5) in plasma and urine determined at 120 min after iv injection of β-[^{18}F]**1** into NMRI-*Foxn1^{nu}* mice breathing either isoflurane/oxygen or isoflurane/air

Tissue	Isoflurane/oxygen	Isoflurane/air
Plasma	91 ± 10	89 ± 8
Urine	97 ± 1	95 ± 1

imaging (MRI) was performed approximately 10 days after tumor inoculation. At this time point tumor growth declined and external necrosis became visible, suggesting the presence of hypoxic regions surrounding the necrotic core within the tumor. Each individual mouse was scanned according to the following imaging schedule: static [^{18}F]FDG and T_1 weighted MRI on the first study day, dynamic PET after injection of β-[^{18}F]**1** under isoflurane/oxygen atmosphere on day 2 and dynamic PET under isoflurane/air anesthesia on the last study day. In all acquired MR images, tumor necrosis was clearly visible as area of low contrast in the tumor center (Fig. 3B). [^{18}F]FDG distribution generally matched this pattern with low radioactivity uptake in MRI-hypointense areas (Fig. 3A). Tumor [^{18}F]FDG uptake was comparable in all studied animals (mean SUV_{max25} = 7.4 ± 1.4, n = 4) suggesting a comparable level of glycolytic activity in the investigated tumors. Tumoral distribution of β-[^{18}F]**1** showed a clear dependence on the employed breathing protocol with almost no radioactivity retention under isoflurane/oxygen breathing and high radioactivity retention under isoflurane/air breathing (Fig. 3C and D).

Time-activity curves of β-[^{18}F]**1** in EMT6 tumors and muscle tissue are shown in Figure 4. Muscle tissue was used as reference tissue as its tissue oxygenation is generally considered to be in the normal physiological range.[38] Under both breathing conditions maximum radioactivity uptake in muscle tissue was reached within the first 10 min after injection followed by a continuous decrease over time. In isoflurane/oxygen breathing animals, elimination of β-[^{18}F]**1** from EMT6 tumors followed the same pattern as muscle tissue. In oxygen/air breathing animals, on the other hand, radioactivity was retained in tumor relative to muscle tissue at time points >60 min after radiotracer injection. Tumor-to-muscle radioactivity ratios increased continuously from 60 min to 120 min after injection under isoflurane/oxygen breathing and remained stable under isoflurane/air breathing (Fig. 4C). Blood

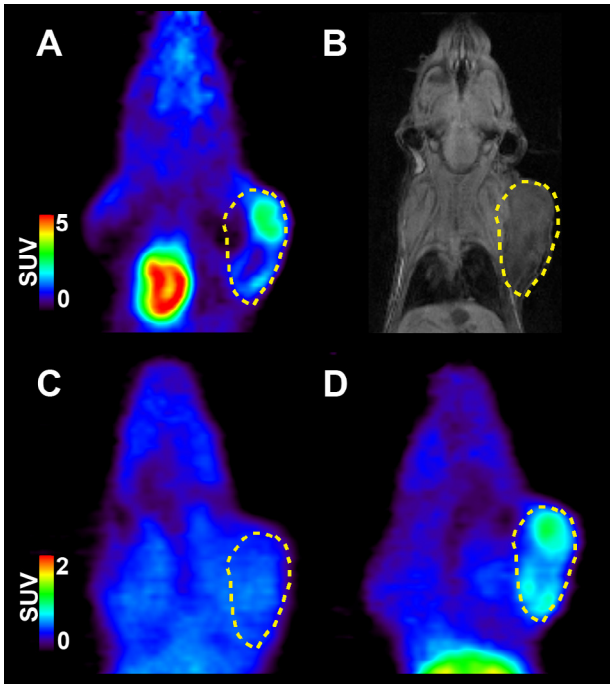

Figure 3. Representative coronal PET summation and MR images of an EMT6 tumor-bearing NMRI-*Foxn1*^{nu} mouse. (A) 60 min after injection of [^{18}F]FDG and (B) T_1 weighted-gradient echo images of corresponding tumor plane. (C) 60–120 min after injection of β-[^{18}F]**1** under isoflurane/oxygen and (D) 60–120 min after injection of β-[^{18}F]**1** under isoflurane/air. Radiation scale is expressed as standardized uptake value (SUV). Yellow dotted line highlights tumor area.

radioactivity concentrations measured at the end of the PET scan were not significantly different between both study groups (mean SUV isoflurane/oxygen = 0.30 ± 0.06; isoflurane/air = 0.38 ± 0.1; n = 4; Fig. 4D).

Tumor-to-muscle (Fig. 5A) and tumor-to-blood ratios (Fig. 5B) at 120 min after injection were significantly higher under isoflurane/air compared to isoflurane/oxygen breathing (tumor-to-muscle ratio: 2.13 ± 0.22 vs 1.22 ± 0.13, p = 0.009; tumor-to-blood ratio: 2.79 ± 0.33 vs 1.84 ± 0.04, p = 0.013; paired 2-tailed t-test). Tumor-to-muscle ratios at 2 h after injection of β-[^{18}F]**1** were in the same range as reported for [^{18}F]FMISO (3.22 ± 0.22) and lower than reported for α-5′-[^{18}F]FAZA (7.10 ± 2.91) in EMT6 bearing BALB/c mice.[16] However, these values were determined at 3 h after radiotracer injection. Moreover, a different anesthesia protocol (ketamine/xylazine) was used, which has been shown to result in increased tumoral retention of α-5′-[^{18}F]FAZA in CT26 tumor xenografted mice compared to isoflurane anesthesia.[34] It seems noteworthy that tumor-to-muscle ratios of β-[^{18}F]**1** increased over time, whereas those of α-5′-[^{18}F]FAZA were shown to decrease over time.[33] This points to irreversible tumor trapping of β-[^{18}F]**1** and suggests that higher tumor-to-muscle ratios might be obtained for β-[^{18}F]**1** than for α-5′-[^{18}F]FAZA at late imaging time points. This assumption remains to be proven in future comparative studies.

2.6. Autoradiography and immunohistochemistry studies

To further confirm the hypoxia specific distribution of β-[^{18}F]**1** in tumor tissue, ex vivo autoradiography studies were conducted in EMT6 tumor bearing mice at 2 h after combined injection of the validated immunohistochemical hypoxia marker pimonidazole and β-[^{18}F]**1**.[39] Distribution of β-[^{18}F]**1** in EMT6 tumor slices followed a heterogeneous pattern with only background uptake in necrotic areas whereas intense retention was found in areas surrounding the necrotic core (Fig. 6). Hematoxylin and eosin staining showed large pale areas suggesting the presence of coagulation necrosis due to occlusion of blood supply. Whole tumor distribution of β-[^{18}F]**1** closely matched that of hypoxia positive pimonidazole staining, which further providing evidence that β-[^{18}F]**1** accumulates in tissues under hypoxic conditions.

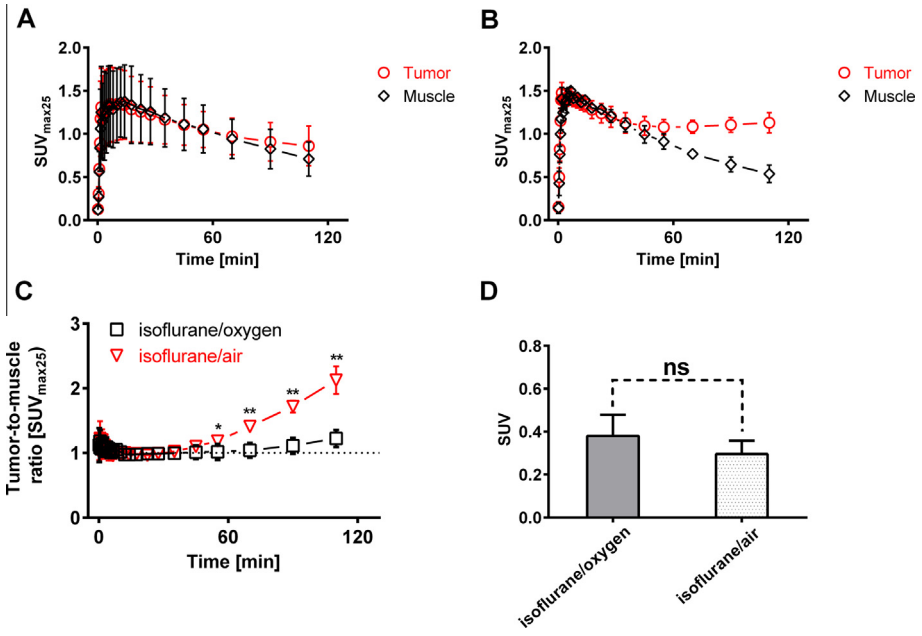

Figure 4. Tissue uptake of β-[^{18}F]**1** over time. Time-activity curves of β-[^{18}F]**1** in tumor (○) and muscle (◇) tissue of EMT6 tumor-bearing NMRI-*Foxn1*^{nu} mice breathing (A) isoflurane/oxygen or (B) isoflurane/air. Tissue radioactivity concentration is expressed as SUV_{max25} meaning that only voxels with values ⩾ 75% of the maximum SUV were used for quantitation. (C) Tumor-to muscle ratios over time in isoflurane/oxygen (□) and isoflurane/air (▽) breathing animals. (D) Total radioactivity concentration in blood measured at the end of the PET scan. Data are mean ± SD for n = 4 animals. ($^{*}p$ <0.05; $^{**}p$ <0.01; ns, not significant; paired 2-tailed t-test).

Please cite this article in press as: Wanek, T.; et al. *Bioorg. Med. Chem.* (2016), http://dx.doi.org/10.1016/j.bmc.2016.08.053

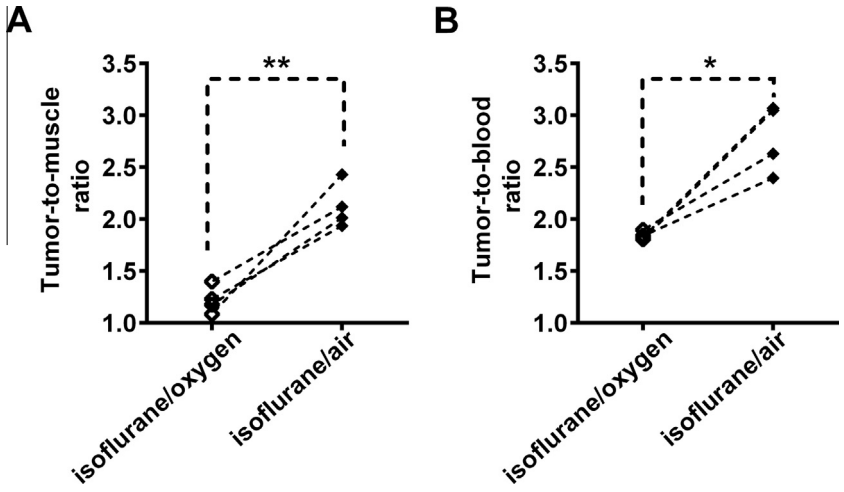

Figure 5. Individual tumor-to-muscle (A) and tumor-to-blood (B) ratios at 2 h post injection of β-[^{18}F]**1** in EMT6 tumor-bearing NMRI-*Foxn1*^{nu} mice (n = 4) breathing either isoflurane/oxygen or isoflurane/air. $^{*}p$ <0.05; $^{**}p$ <0.01 (paired 2-tailed t-test).

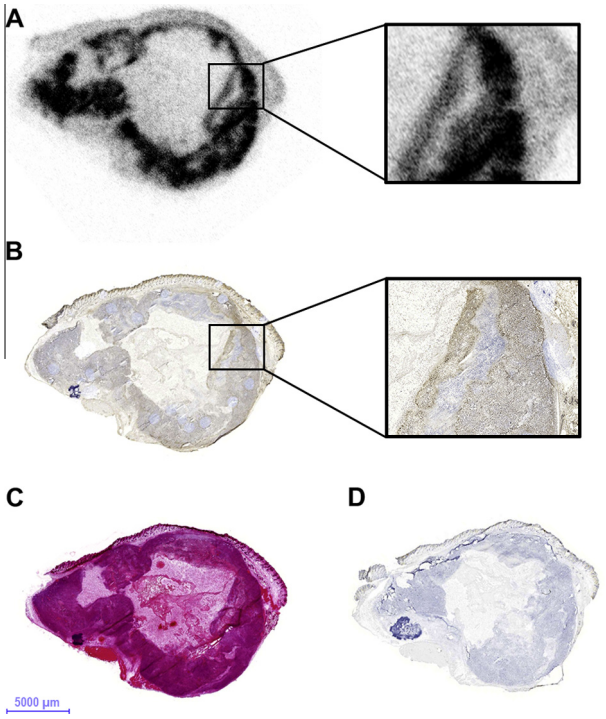

Figure 6. Ex vivo microtumoral distribution pattern of β-[^{18}F]**1** matches with pimonidazole immunohistochemistry in corresponding EMT6 tumor slices. (A) autoradiographic image of β-[^{18}F]**1** distribution in EMT6 tumor tissue 2 h post injection, (B) pimonidazole stain, (C) histologic (H&E) stain and (D) negative control of pimonidazole stain. Box inlay shows 10× magnification of the indicated area.

3. Conclusions

We described the radiosynthesis of the ^{18}F-labeled 2-nitroimidazole derivative β-[^{18}F]**1** as a potential hypoxia specific PET tracer, which shows interaction with human nucleoside transporters suggesting that uptake of β-[^{18}F]**1** into tumor cells is mediated. β-[^{18}F]**1** was shown to have hypoxia sensitive uptake in murine and human tumor cell lines. In vivo studies showed a fast and homogenous distribution of β-[^{18}F]**1** in healthy tissues and negligible radiotracer metabolism. PET studies revealed high tumor-to-muscle ratios within 2 h after injection and the use of different breathing protocols confirmed an oxygen sensitive uptake in tumor tissue. Microtumoral distribution of β-[^{18}F]**1** studied with ex vivo autoradiography closely matched that of pimonidazole, a validated marker for tumor hypoxia. These data suggest that β-[^{18}F]**1** might be a suitable radiotracer for noninvasive imaging of hypoxia with PET. Further in vivo studies to compare β-[^{18}F]**1** with other hypoxia radiotracers seem justified.

4. Experimental section

4.1. General

Unless otherwise stated, all chemicals were of analytical grade and obtained from Sigma–Aldrich Chemie GmbH (Schnelldorf, Germany), Acros (distributed by Fisher Scientific, Schwerte, Germany) or Merck (Darmstadt, Germany) and used without further purification. 1,2:5,6-Di-*O*-isopropylidene-α-D-allofuranose was obtained from Carbosynth Limited (Compton, UK). Isoflurane was obtained from Abbott Laboratories Ltd. (Maidenhead, UK). All cell culture media (Waymouth's MB752/1, RPMI) as well as heat inactivated fetal bovine serum (FBS), penicillin/streptomycin solution, phosphate buffered saline (PBS) and trypsin–EDTA solution were purchased from Gibco (Invitrogen, Lofer, Austria). [^{18}F]Fluoride was produced in a PETtrace cyclotron (GE Healthcare, Uppsala, Sweden) by irradiation of 2.6 mL enriched [^{18}O]water (Rotem, Arava, Israel, ⩾97% enrichment) via the ^{18}O(p,n)^{18}F nuclear reaction. For tracer production, irradiations were performed for durations of 80 ± 20 min with a mean beam current of 50 ± 7 μA yielding 140 ± 30 GBq fluorine-18 at end of beam. [^{18}F]FDG was purchased from Seibersdorf Labor GmbH (Seibersdorf, Austria). [^{3}H]Uridine (specific activity: 185–555 GBq/mmol) was purchased from Moravek Biochemicals (Brea, CA, USA). Pimonidazole hydrochloride (1-[(2-hydroxy-3-piperidinyl)propyl]-2-nitroimidazole hydrochloride) and rabbit anti-pimonidazole antibody were obtained from Hypoxyprobe Inc. (Burlington, MA, USA). Donkey-anti rabbit secondary antibody was purchased from Jackson ImmunoResearch (West Grove, PA, USA). Antibody diluent and serum-free protein block solution were acquired from Dako (Glostrup, Denmark). Avidin–biotin–peroxidase complex (Vectastain) was purchased from Vector Laboratories Inc. (Burlingame, CA, USA). ^{1}H and ^{13}C (*J*-modulated) NMR spectra were recorded on a Bruker Avance AVIII 400 (^{1}H: 400.27 MHz, ^{13}C: 100.65 MHz), AV 400 (^{1}H: 400.31 MHz, ^{13}C: 100.61 MHz) or DRX 600 (^{1}H: 600.13 MHz, ^{13}C: 150.90 MHz)

spectrometer in $CDCl_3$ unless otherwise stated. Chemical shifts are reported in δ units (ppm) and were referenced to residual $CHCl_3$ (δ_H 7.24), $CDCl_3$ (δ_C 77.00), residual DMSO-d_5 (δ_H 2.50) or DMSO-d_6 (δ_C 39.50). *J* values are reported in Hertz. IR spectra were recorded on a Bruker VERTEX 70 IR spectrometer (Bruker, Billerica, MA, USA) or of films on a silicon disc on a Perkin Elmer 1600 FT-IR spectrometer (Perkin Elmer, Waltham, MA, USA). Optical rotations were measured at 20 °C on a Perkin Elmer 351 polarimeter in a 10 cm cell. Melting points were determined on a Reichert Thermovar instrument (Reichert Technologies, Depew, NY, USA) and are uncorrected.

Flash (column) chromatography was performed with Merck silica gel 60 (230–400 mesh). TLC was carried out on 0.25 mm thick Merck silica gel 60 F_{254} plates. Spots were visualized by UV and/or dipping the plate into a solution of $(NH_4)_6Mo_7O_{24}{\cdot}4H_2O$ (23.0 g) and $Ce(SO_4)_2{\cdot}4H_2O$ (1.0 g) in 10% aqueous H_2SO_4 (500 mL), followed by heating with a heat gun.

Pyridine was dried by refluxing over powdered CaH_2, then distilled and stored over molecular sieves (4 Å). Dichloromethane was dried by passing through aluminum oxide 90 active neutral (0.063–0.200 mm, activity I) and stored over molecular sieves (3 Å).

4.2. Cell lines

Mouse mammary carcinoma cells EMT6 (CRL-2755) and the human non-small cell lung cancer cell line NCI-H1975 (CRL-5908) were obtained from the American Type Culture Collection (ATCC, Manassas, VA, USA). EMT6 cells were cultured as monolayers in Waymouth's medium supplemented with 15% fetal bovine serum (FBS) and 0.1 mg/mL penicillin/streptomycin solution (10.000 U/mL). NCI-H1975 cells were maintained in RPMI 1640 medium with 10% FBS, 2 mM L-glutamine and 0.1 mg/mL penicillin/streptomycin. All cell lines were passaged twice per week and maintained at 37 °C and 5% CO_2 prior to use for experiments.

4.3. Animals

Female athymic nude NMRI-Foxn1^{nu} mice were obtained from Taconic (Lille Skensved, Denmark) and housed in groups (4–6 animals) in polysulfon type III cages under individual ventilated cage conditions. The environmental conditions were as follows: temperature, 22 ± 3 °C; humidity, 40% to 70%; and a 12 h light/dark cycle (lights on at 06:00) with free access to autoclaved standard laboratory rodent diet (ssniff R/M-H, ssniff Spezialdiäten GmbH, Soest, Germany) and sterile tap water. An acclimatization period of at least one week was allowed before the animals were used in the experiments. All animal experiments were approved by the national authorities (Amt der Niederösterreichischen Landesregierung), and all study procedures were performed in accordance with the European Communities Council Directive of September 22, 2010 (2010/63/EU). All efforts were made to comply with the 3Rs principle in this study.

4.4. Synthesis of precursor

4.4.1. 3-*O*-Acetyl-1,2-*O*-isopropylidene-α-D-allofuranose (2)

1,2:5,6-Di-*O*-isopropylidene-α-D-allofuranose was acetylated according to a published procedure.[25] The analytical sample was crystallized from hexanes; mp 75–76 °C (lit. 25 77–78 °C). The crude product (94%) was pure enough for the next step, the removal of the 5,6-isopropylidene group with 60% AcOH. The crude product was purified by flash chromatography using hexanes/EtOAc (1:2, R_f = 0.23) to yield **2** (6.12 g, 85% for both steps) as a colorless syrup.

4.4.2. 3-*O*-Acetyl-1,2-*O*-isopropylidene-6-*O*-*p*-toluenesulfonyl-α-D-allofuranose (3)

A solution of **2** (5.25 g, 20 mmol) and *p*-toluenesulfonyl chloride (3.82 g, 20 mmol) in dry pyridine (23.73 g, 300 mmol, 24.16 mL) was kept at -25 °C for 40 h. Water (20 mL) was added and after stirring for 15 min the mixture was extracted with CH_2Cl_2 (3 × 20 mL). The combined organic phases were washed with 4 M HCl until the pyridine was removed (monitored by TLC), water and saturated aqueous solution of $NaHCO_3$, dried (Na_2SO_4) and concentrated under reduced pressure. The crude product was purified by flash chromatography using hexanes/EtOAc (2:1, R_f = 0.18) to give monotosylate **3** (6.15 g, 74%) as a crystalline solid; mp 111–113 °C (hexanes/1,2-$C_2H_4Cl_2$), $[\alpha]_D^{20}$ +82.31 (*c* 1.47, acetone). Virtually no ditosylate could be detected. ^{1}H NMR (400.27 MHz, $CDCl_3$): δ 7.80–7.75 (m, 2H), 7.36–7.31 (m, 2H), 5.74 (d, *J* = 3.7 Hz, 1H), 4.83 (dd, *J* = 8.4, 4.9 Hz, 1H), 4.79 (dd, *J* = 4.9, 3.7 Hz, 1H), 4.16 (dd, *J* = 10.1, 3.4 Hz, 1H), 4.10 (dd, *J* = 8.4, 4.6 Hz, 1H) 4.07–4.02 (m, 1H), 3.97 (dd, *J* = 10.1, 6.8 Hz, 1H), 2.44 (s, 3H), 2.34 (br. s, 1H), 2.09 (s, 3H), 1.52 (s, 3H), 1.31 (s, 3H). ^{13}C NMR (100.65 MHz, $CDCl_3$): δ 170.2, 145.1, 132.6, 130.0 (2C), 128.0 (2C), 113.4, 104.1, 77.7, 77.1, 72.3, 70.1, 69.4, 26.7 (2C), 21.6, 20.7. IR (Si): ν 3491, 2988, 1744, 1372, 1243, 1177, 1028, 983, 913 cm^{-1}. Anal. Calcd for $C_{18}H_{24}O_9S$ (416.44): C, 51.91; H, 5.81; S, 7.70. Found: C, 51.94; H, 5.84; S, 7.60.

4.4.3. 3,5-Di-*O*-acetyl-1,2-*O*-isopropylidene-6-*O*-*p*-toluenesulfonyl-α-D-allofuranose (4)

A mixture of monotosylate **3** (6.15 g, 14.77 mmol), Ac_2O (3.02 g, 2.80 mL, 29.6 mmol) and dry pyridine (3.50 g, 3.58 mL, 44.4 mmol) in dry CH_2Cl_2 (7.5 mL) was stirred at 40 °C for 2.5 h and then cooled to rt. Water (20 mL) was added and after stirring for 10 min the mixture was extracted with CH_2Cl_2 (3 × 20 mL). The combined organic phases were washed with 2 M HCl (2 × 20 mL), water and saturated aqueous solution of $NaHCO_3$, dried (Na_2SO_4) and concentrated under reduced pressure. The crude product which was a very viscous oil (quantitative yield) was pure enough for the subsequent reaction. The analytical sample was crystallized from CH_2Cl_2/iPr_2O to yield diacetate **4** as colorless crystals; mp 76–77 °C, $[\alpha]_D^{20}$ +74.81 (*c* 1.04, acetone). ^{1}H NMR (400.27 MHz, $CDCl_3$): δ 7.77–7.74 (m, 2H), 7.35–7.31 (m, 2H), 5.70 (d, *J* = 3.6 Hz, 1H), 5.12 (td, *J* = 5.8, 3.6 Hz, 1H), 4.77 (dd, *J* = 5.0, 3.6 Hz, 1H), 4.73 (dd, *J* = 8.5, 5.0 Hz, 1H), 4.20 (dd, *J* = 8.6, 5.8 Hz, 1H), 4.18 (ABX sys, J_{AB} = 11.0 Hz, J_{AX} = 3.6 Hz, J_{BX} = 5.8 Hz, 2H), 2.43 (s, 3H), 2.10 (s, 3H), 1.99 (s, 3H), 1.52 (s, 3H), 1.30 (s, 3H). ^{13}C NMR (100.65 MHz, $CDCl_3$): δ 169.8, 169.6, 145.0, 132.7, 129.9, 127.9, 113.4, 104.0, 77.4, 75.3, 73.5, 70.1, 67.4, 26.6 (2C), 21.6, 20.6, 20.5. IR (Si): ν 2990, 1750, 1374, 1243, 1178, 1025 cm^{-1}. Anal. Calcd for $C_{20}H_{26}O_{10}S$ (458.48): C, 52.39; H, 5.72. Found: C, 52.33; H 5.69.

4.4.4. 1,2,3,5-Tetra-*O*-acetyl-6-*O*-*p*-toluenesulfonyl-α- and 1,2,3,5-tetra-*O*-acetyl-6-*O*-*p*-toluenesulfonyl-β-D-allofuranose (α- and β-5)

A mixture of diacetate **4** (2.94 g, 6.4 mmol) and 60% aqueous TFA (12.84 mL) was stirred for 40 min at rt. Water (20 mL) was added and the product was extracted with ethyl acetate (3 × 20 mL). The combined organic phases were washed with a saturated aqueous solution of $NaHCO_3$ until neutral, dried (Na_2SO_4) and concentrated under reduced pressure. After drying the gum at 1 mbar dry CH_2Cl_2 (13 mL), Ac_2O (2.62 g, 2.43 mL, 25.7 mmol), and dry pyridine (4.06 g, 4.12 mL, 51.3 mmol) were added. The mixture was stirred at 40 °C for 2.5 h. Water (20 mL) was added and the mixture was extracted with CH_2Cl_2 (3 × 20 mL). The combined organic phases were washed with 2 M HCl (20 mL), water and saturated aqueous solution of $NaHCO_3$, dried (Na_2SO_4) and concentrated under reduced pressure. The residue was purified by flash

chromatography using hexanes/EtOAc (1:1, α: R_f = 0.53, β: R_f = 0.43) to yield a mixture of tetraacetates α- and β-5 (2.522 g, 78%) as a gum; α/β = 3:1 (by ^{1}H NMR); $[\alpha]_D^{20}$ +6.11 (*c* 1.44, acetone).

A homogenous sample of α-anomer α-**5** (R_f = 0.53) was obtained by flash chromatography as a gum. Crystallization from CH_2Cl_2/iPr_2O gave crystals containing 0.41 mol of EtOAc (by ^{1}H NMR) after drying at rt/1 mbar; melting range 48–55 °C. $[\alpha]_D^{20}$ −7.48 (*c* 1.03, acetone).

α-Anomer α-**5**; gum, $[\alpha]_D^{20}$ −10.0 (*c* 1.02, acetone): ^{1}H NMR (600.13 MHz, $CDCl_3$): δ 7.77–7.73 (m, 2H), 7.35–7.32 (m, 2H), 6.09 (d, *J* = 0.7 Hz, 1H), 5.43 (dd, *J* = 6.7, 5.0 Hz, 1H), 5.27 (dd, *J* = 5.0, 0.7 Hz, 1H), 5.00 (ddd, *J* = 7.0, 4.5, 3.2 Hz, 1H), 4.31 (dd, *J* = 7.0, 6.7 Hz, 1H), 4.24 (dd, *J* = 11.3, 3.2 Hz, 1H), 4.09 (dd, *J* = 11.3, 4.5 Hz, 1H), 2.43 (s, 3H), 2.11 (s, 3H), 2.044 (s, 3H), 2.042 (s, 3H), 1.98 (s, 3H). ^{13}C NMR (150.90 MHz, $CDCl_3$): δ 169.6, 169.33, 169.32, 168.7, 145.2, 132.5, 129.9 (2C), 128.0 (2C), 98.2, 78.7, 74.3, 71.1, 71.0, 67.3, 21.7, 21.0, 20.6, 20.5, 20.4. IR (Si): *ν* 3005, 2970, 1740, 1436, 1366, 1228, 1217 cm^{-1}. Anal. Calcd for $C_{21}H_{26}O_{12}S$ (502.49): C, 48.72; H, 5.03. Found: C, 48.61; H, 5.03 for compound with 0.41 iPr_2O.

*Mixture of anomers α- and β-***5** (α/β = 3:1), contained 5–10% of an impurity; ^{1}H NMR (400.27 MHz, $CDCl_3$), only signals of β-anomer are given as those of the α-anomer are identical to those given for the homogenous α-anomer above: δ 7.78–7.71 (m, 2H), 7.36–7.29 (m, 2H), 6.30 (d, *J* = 4.5 Hz, 1H), 5.37 (dd, *J* = 6.9, 3.1 Hz, 1H), 5.08 (dd, *J* = 6.9, 4.5 Hz, 1H), 5.03–4.97 (m, 1H), 4.39 (dd, *J* = 4.5, 3.1 Hz, 1H), 4.15 (AB part of ABX system, J_{AB} = 11.3 Hz, *J* = 4.4, 4.0 Hz, 2H), 2.43 (s, 3H), 2.10 (s, 3H), 2.08 (s, 3H), 2.02 (s, 3H), 1.99 (s, 3H). ^{13}C NMR (100.65 MHz, $CDCl_3$): only signals of β-anomer β-**5** are given, for those of α-anomer see above: δ 169.7, 169.6, 169.4, 169.2, 145.2, 132.4, 130.0 (2C), 128.0 (2C), 93.4, 81.4, 69.7, 69.6, 68.6, 67.1, 21.6, 20.9, 20.6, 20.5, 21.2. Anal. Calcd for $C_{21}H_{26}O_{12}S$ (502.49): C, 50.19; H, 5.22. Found: C, 49.98; H, 5.25.

4.4.5. 1-(2′,3′,5′-Tri-*O*-acetyl-6′-*O*-*p*-toluenesulfonyl-α- and (2′,3′,5′-tri-*O*-acetyl-6′-*O*-*p*-toluenesulfonyl-β-D-allofuranosyl)-2-nitroimidazole (α- and β-6)

A mixture of 2-nitroimidazole (0.134 g, 1.19 mmol), hexaethyldisilazane (0.583 g, 2.38 mmol) and dry pyridine (2.0 mL) was refluxed for 30 min.[31] After cooling to rt, volatiles were removed by bulb to bulb distillation at 0.7 mbar (final temperature 90 °C). Dry CH_3CN (4.0 mL) and a solution of tetraacetates α- and β-5 (α/β = 3:1) (0.543 g, 1.08 mmol) in dry CH_3CN (6 mL) were added to the crystalline residue under argon atmosphere. The mixture was ultrasonicated for 5 min before the addition of a solution of $TfOSiEt_3$ (1.296 mL, 1 M in dry 1,2-$C_2H_4Cl_2$) at 0 °C. After 1 h (TLC control) the reaction was quenched with a saturated aqueous solution of $NaHCO_3$ (10 mL). The mixture was extracted with EtOAc (3 × 10 mL). The combined organic layers were washed with a mixture of water and brine (5 mL each), dried (Na_2SO_4) and concentrated under reduced pressure. The residue (^{1}H NMR: α-6/β-6/α-5/β-5 = 0.04:1.00:0.05:0.05) was flash chromatographed using CH_2Cl_2/EtOAc (7:1, α: R_f = 0.43; β: R_f = 0.33) to yield anomers α-6 (0.029 g, 5%) and β-6 (0.266 g, 44%) as foams.

α-Anomer α-**6**: $[\alpha]_D^{20}$ −43.14 (*c* 1.02, acetone); it could not be induced to crystallize. ^{1}H NMR (400.13 MHz, $CDCl_3$): δ 7.79–7.74 (m, 2H), 7.37 (d, *J* = 1.2 Hz, 1H), 7.36–7.32 (m, 2H), 7.19 (d, *J* = 1.2 Hz, 1H), 6.79 (d, *J* = 5.3 Hz, 1H), 5.76 (t, *J* = 5.3 Hz, 1H), 5.49 (dd, *J* = 5.3, 4.0 Hz, 1H), 5.08 (td, *J* = 6.1, 4.0 Hz, 1H), 4.70 (dd, *J* = 6.1, 4.0 Hz, 1H), 4.23 (AB part of ABX system, J_{AB} = 11.3 Hz, $J_{AX} \approx J_{BX}$ = 4.0 Hz, 2H), 2.44 (s, 3H), 2.05 (s, 3H), 1.94 (s, 3H), 1.85 (s, 3H). ^{13}C NMR (150.90 MHz, $CDCl_3$): δ 169.5, 168.9, 168.1, 145.5, 144.4, 132.2, 130.1 (2C), 128.0 (2C), 127.9, 122.5, 87.2, 81.1, 70.3, 70.2, 69.9, 66.6, 21.7, 20.7, 20.2, 19.8. IR (ATR): *ν* 1752, 1540, 1480, 1365, 1219, 1177 cm^{-1}. Anal. Calcd for $C_{22}H_{25}N_3O_{12}S$ (555.51): C, 47.57; H, 4.54; N, 7.56. Found: C, 47.37; H, 4.48; N, 7.43.

β-Anomer β-**6**: More polar than α-anomer. It was crystallized from EtOAc/iPr_2O by slowly cooling from +25 °C to −17 °C to give light yellowish needles, which were dried for 1 h at rt/1 mbar, contained 0.50 mol of EtOAc (by ^{1}H NMR); when kept in vacuum (5 h/rt/0.8 mbar), the ratio changed from 1.00:0.50 to 1.00:0.45; mp 71–72 °C; $[\alpha]_D^{20}$ +27.10 (*c* 1.07, acetone). ^{1}H NMR (400.13 MHz, $CDCl_3$): δ 7.77–7.72 (m, 2H), 7.36–7.30 (m, 2H), 7.24 (s, 1H), 7.17 (s, 1H), 6.54 (d, *J* = 4.2 Hz, 1H), 5.40 (AB part of ABXY system, J_{AB} = 5.7 Hz, *J* = 5.6, 4.2 Hz, 2H), 5.22 (td, *J* = 5.6, 4.2 Hz, 1H), 4.39 (t, *J* = 5.6 Hz, 1H), 4.19 (AB part of ABX system, J_{AB} = 11.3 Hz, J_{AX} = J_{BX} = 4.2 Hz, 2H), 2.43 (s, 3H), 2.10 (s, 3H), 2.09 (s, 3H), 2.02 (s, 3H). Signals of EtOAc: 4.09 (q, *J* = 7.0 Hz, 2H), 2.02 (s, 3H), 1.23 (t, *J* = 7.0 Hz, 3H). ^{13}C NMR (100.65 MHz, $CDCl_3$, not jmod): δ 169.5, 169.2, 169.0, 145.5, 144.4, 132.2, 130.0 (2C), 129.1, 128.0 (2C), 121.1, 88.7, 79.5, 74.4, 69.7, 69.3, 66.6, 21.7, 20.6, 20.4, 20.3. Signals for EtOAc are not given. IR (ATR, crystals): *ν* 2914, 1755, 1739, 1548, 1484, 1358, 1230, 1178, 1075 cm^{-1}. Anal. Calcd for $C_{22}H_{25}N_3O_{12}S \times 0.50$ EtOAc = $C_{24}H_{29}N_3O_{13}S$ (599.56): C, 48.08; H, 4.88; N, 7.01; O, 34.69; S 5.35. Found: C, 48.04; H, 4.83; N, 7.10; S, 5.39.

4.5. Synthesis of reference compound

4.5.1. 1,2-*O*-Isopropylidene-α-D-allofuranose (7)

A mixture of 1,2:5,6-di-*O*-isopropylidene-α-D-allofuranose (6.51 g, 25 mmol) and 60% aqueous AcOH (75 mL) was stirred at rt for 18 h. The solution was then concentrated under reduced pressure and coevaporated with toluene (2 × 10 mL). The crude product was purified with flash chromatography using EtOAc/ethanol (10:1, R_f = 0.28) to yield triol **7** (4.21 g, 77%) as colorless crystals. The analytical sample was crystallized from EtOAc, mp 128–129 °C (lit. 40 129–130 °C). ^{1}H NMR (400.27 MHz, $CDCl_3$): δ 5.80 (d, *J* = 3.8 Hz, 1H), 4.62 (dd, *J* = 5.0, 3.8 Hz, 1H), 4.11 (td, *J* = 8.4, 5.0 Hz, 1H), 4.02 (∼quint, *J* = 3.5 Hz, 1H), 3.84 (dd, *J* = 8.4, 3.3 Hz, 1H), 3.89–3.74 (m, 2H), 3.16 (d, *J* = 8.4 Hz, 1H), 2.51 (br t, *J* = 6.0 Hz, 1H), 2.47 (d, *J* = 3.5 Hz, 1H), 1.57 (s, 3H), 1.36 (s, 3H). ^{13}C NMR (100.65 MHz, $CDCl_3$): δ 113.1, 103.9, 81.1, 79.0, 70.3, 70.2, 62.9, 26.6, 26.4.

4.5.2. 5,6-Anhydro-1,2-*O*-isopropylidene-α-D-allofuranose (8)

A mixture of triol **7** (4.215 g, 19.14 mmol), diisopropyl azodicarboxylate (DIAD) (4.645 g, 4.52 mL, 22.97 mmol) and triphenylphosphane (6.024 g, 22.97 mmol) in dry toluene (115 mL) was refluxed for 5 h. The solution was concentrated under reduced pressure. The residue was purified by flash chromatography using hexanes/EtOAc (10:1, TLC: hexanes/EtOAc, 1:1, R_f = 0.39) to yield anhydroallofuranose **8** (3.436 g, 89%) as colorless crystals. The analytical sample was recrystallized from iPr_2O; mp 65–67 °C, $[\alpha]_D^{20}$ +61.78 (*c* 1.07, acetone). ^{1}H NMR (400.13 MHz, $CDCl_3$): δ 5.81 (d, *J* = 3.9 Hz, 1H), 4.54 (dd, *J* = 5.2, 3.9 Hz, 1H), 3.94 (dd, *J* = 8.6, 2.8 Hz, 1H), 3.80 (ddd, *J* = 10.6, 8.6, 5.2 Hz, 1H), 3.27 (td, *J* = 4.0, 2.8 Hz, 1H), 2.82 (ABX sys, *J* = 5.1, 4.0, 2.8 Hz, 2H), 2.35 (d, *J* = 10.6 Hz, 1H), 1.55 (s, 3H), 1.35 (s, 3H). ^{13}C NMR (100.61 MHz, $CDCl_3$): δ 112.7, 103.9, 79.3, 78.4, 70.8, 50.1, 43.9, 26.6, 26.5, IR (ATR, solid): *ν* 3528, 2980, 1376, 1240, 1169, 1124, 1066, 1034, 992 cm^{-1}. Anal. Calcd for $C_9H_{14}O_5$ (202.20): C, 53.46; H, 6.98. Found: C, 53.45; H, 6.93.

4.5.3. 3,5-Di-*O*-acetyl-6-deoxy-6-fluoro-1,2-*O*-isopropylidene-α-D-allofuranose (9)

40% HF (0.464 ml, 10.68 mmol) was added to TBAF (10.68 mL, 10.68 mmol, 1 M in THF) and after 5 min the solution was concentrated under reduced pressure. After the residue had been dried

under reduced pressure (1 mbar, 100 °C, 1 h), anhydroallofuranose **8** (0.72 g, 3.56 mmol), KHF_2 (0.086 g, 1.07 mmol) and dry toluene (7 mL) were added and the mixture was heated (oil bath temperature 120 °C) for 18 h. After cooling to rt, Ac_2O (1.453 g, 1.35 mL, 14.24 mmol) and dry pyridine (2.253 g, 2.30 mL, 28.48 mmol) were added. The mixture was stirred at 40 °C for 2 h. Water (10 mL) was added and the product was extracted with ethyl acetate (3 × 10 mL). The combined organic phases were washed with 2 M HCl (10 mL), water and saturated aqueous solution of $NaHCO_3$, dried (Na_2SO_4) and concentrated under reduced pressure. The residue was purified by flash chromatography using hexanes/EtOAc (1:1, R_f = 0.63) to yield diacetate **9** (0.93 g, 86%) as colorless oil; $[\alpha]_D^{20}$ +148.73 (*c* 0.985, acetone). ^{1}H NMR (400.27 MHz, $CDCl_3$): δ 5.77 (d, J = 3.6 Hz, 1H), 5.22 (tdd, J_{HF} = 21.1 Hz, J = 5.1, 3.6 Hz, 1H), 4.84–4.77 (m, 2H, 2-H), 4.55 (AB part of ABX sys. coupling with fluorine, J_{HF} = 46.8 Hz J_{AB} = 10.3 Hz, J = 5.1, 3.6 Hz, 2H), 4.30–4.24 (m, 1H), 2.11 (s, 3H), 2.08 (s, 3H), 1.53 (s, 1H), 1.12 (s, 3H). ^{13}C NMR (100.65 MHz, $CDCl_3$): δ 170.0 (d, J_{CF} = 3.8 Hz), 113.4, 104.1, 81.0 (d, J_{CF} = 173.6 Hz), 77.4, 75.2 (d, J_{CF} = 5.9 Hz), 73.4, 71.1 (d, J_{CF} = 19.3 Hz), 26.6 (2C), 20.8, 20.6. IR (ATR): ν 1743, 1374, 1217, 1071, 1017 cm^{-1}. Anal. Calcd for $C_{13}H_{19}FO_7$ (306.28): C, 50.98; H, 6.25. Found: C, 50.72; H 6.24.

4.5.4. 1,2,3,5-Tetra-*O*-acetyl-6-deoxy-6-fluoro-α- and 1,2,3,5-tetra-*O*-acetyl-6-deoxy-6-fluoro-β-D-allofuranose (α- and β-10)

A mixture of diacetate **9** (1.19 g, 3.88 mmol) and 60% aqueous TFA (7.76 mL) was stirred for 25 min and subsequently concentrated under reduced pressure. The residue was dried by coevaporation with toluene (2×) and after drying under vacuum (1 mbar, 40 °C, 1 h), Ac_2O (1.58 g, 1.47 mL, 15.52 mmol), dry pyridine (2.51 g, 2.49 mL, 31.04 mmol) and dry CH_2Cl_2 (8 mL) were added and the mixture was stirred at 40 °C for 1.5 h. After cooling water (10 mL) was added and stirring was continued for 10 min. The mixture was extracted with CH_2Cl_2 (3 × 15 mL). The combined organic phases were washed with 2 M HCl (2 × 10 mL), water and saturated aqueous solution of $NaHCO_3$, dried (Na_2SO_4) and concentrated under reduced pressure. The residue was purified by flash chromatography using hexanes/EtOAc (2:1, α: R_f = 0.33, β: R_f = 0.19) to yield mixture of anomeric tetraacetates α- and β-**10** (0.95 g, 70%) as a gum; α/β = 3:1 (by ^{1}H NMR); $[\alpha]_D^{20}$ +10.18 (*c* 1.06, acetone). When this experiment was repeated fractions containing only one anomer were pooled to obtain homogenous samples for characterization.

α-Anomer α-***10***: Mp 73–74 °C (*i*Pr_2O); $[\alpha]_D^{20}$ −11.98 (*c* 1.06, acetone). ^{1}H NMR (400.27 MHz, $CDCl_3$): δ 6.16 (d, J = 0.9 Hz, 1H), 5.50 (dd, J = 6.7, 5.0 Hz, 1H), 5.31 (dd, J = 5.0, 0.9 Hz, 1H), 5.10 (dddd, J_{HF} = 23.4 Hz, J = 6.7, 4.0, 3.1 Hz, 1H), 4.56 (AB part of ABX system coupling with F, J_{HF} = 47.1 Hz, J_{AB} = 10.5 Hz, J = 4.0, 3.1 Hz, 2H), 4.36 (t, J = 6.7 Hz, 1H), 2.11 (s, 3H), 2.09 (s, 3H), 2.08 (s, 1H), 2.05 (s, 3H). ^{13}C NMR (100.65 MHz, $CDCl_3$): δ 169.8, 169.4, 169.3, 168.9, 98.4, 81.0 (d, J = 174.0 Hz), 78.9 (d, J = 5.6 Hz), 74.4, 72.1 (d, J = 18.8 Hz), 71.0, 21.0, 20.8, 20.5, 20.4. IR (ATR): ν 2926, 1746, 1372, 1208, 1103, 1085, 1011, 963 cm^{-1}. Anal. Calcd for $C_{14}H_{19}FO_9$ (350.29): C, 48.00; H, 5.44. Found: C, 48.15: H, 5.36.

β-Anomer β-***10***: Colorless oil, contained 5% of α-anomer; $[\alpha]_D^{20}$ +86.69 (*c* 1.315, acetone). ^{1}H NMR (400.27 MHz, $CDCl_3$): δ 6.39 (d, J = 4.5 Hz, 1H), 5.45 (dd, J = 6.8, 2.9 Hz, 1H), 5.16 (dd, J = 6.8, 4.5 Hz, 1H), 5.12 (tdd, J_{HF} = 22.4 Hz, J = 5.1, 4.0 Hz, 1H), 4.57 (dd, J_{HF} = 46.9 Hz, J = 4.0 Hz, 2H), 4.43 (dd, J = 5.1, 2.9 Hz, 1H), 2.113 (s, 3H), 2.112 (s, 3H), 2.10 (s, 3H), 2.04 (s, 3H). ^{13}C NMR (100.61 MHz, $CDCl_3$): δ 169.8, 169.7, 169.5, 169.2, 93.5, 81.6 (d, J = 4.3 Hz), 80.8 (d, J = 173.8 Hz), 70.9 (d, J = 20.0 Hz), 69.8, 21.0, 20.8, 20.6, 20.3. IR (Si): ν 3016, 2970, 1739, 1435, 1366, 1228, 1217 cm^{-1}. Anal. Calcd for $C_{14}H_{19}FO_9$ (350.29): C, 48.00; H, 5.44. Found: C, 48.16; H, 5.44.

4.5.5. 1-(2′,3′,5′-Tri-*O*-acetyl-6′-deoxy-6′-fluoro-*α*- and 2′,3′,5′-tri-*O*-acetyl-6′-deoxy-6′-fluoro-β-D-allofuranosyl)-2-nitroimidazole (α- and β-11)

A mixture of 2-nitroimidazole (0.363 g, 3.2 mmol), hexaethyldisilazane (1.574 g, 6.41 mmol) and dry pyridine (5.3 mL) was refluxed for 20 min. After cooling to rt, volatiles were removed by bulb to bulb distillation at 0.7 mbar (final temperature 90 °C). Dry CH_3CN (11 mL) and a solution of tetraacetates α- and β-10 (α/β = 3:1) (1.02 g, 2.91 mmol) in dry CH_3CN (16 mL) were added to the crystalline residue under argon atmosphere. The mixture was ultrasonicated for 5 min before the addition of a solution of $TfOSiEt_3$ (3.5 mL, 1 M in dry 1,2-$C_2H_4Cl_2$) at 0 °C. After 15 min, when the solid had dissolved, the reaction was quenched with a saturated aqueous solution of $NaHCO_3$ (20 mL) [TLC in CH_2Cl_2/EtOAc 10:1, R_f (α-11, less polar) = 0.41; R_f (β-11, more polar) = 0.31) showed that starting material was still present]. The mixture was extracted with EtOAc (3 × 20 mL). The combined organic layers were washed with a mixture of water and brine (10 mL each), dried (Na_2SO_4) and concentrated under reduced pressure. The residue (^{1}H NMR: α-11/β-11/α-10/β-10 = 1.00:3.86:2.30:0.92) was flash chromatographed using CH_2Cl_2/EtOAc (10:1, α-11: R_f = 0.41, β-11: R_f = 0.31) to yield α-11 (0.090 g, 8%) and β-11 (0.516 g, 44%), both as faint orange crystals.

Similarly, 1 mmol of tetraacetates α- and β-**10** (α/β = 3:1) was reacted with 1 mmol of silylated 2-nitroimidazole and $TfOSiEt_3$ (1 mL, 1 M in dry 1,2-$C_2H_4Cl_2$) at rt for 1.5 h. As there was still starting material present (TLC), another portion of $TfOSiEt_3$ (1 mL) was added. After a combined reaction time of 3 h, the reaction mixture was worked up. The crude product (^{1}H NMR: α-**11**/β-**11**/α-**10**/β-**10** = 1.00:0.13:0.54:0.14) was flash chromatographed to give mixture of anomers α- and β-**11** (0.210 g, 52%).

α-Anomer α-***11***: Less polar than β-anomer β-**11**, mp 145–146 °C ($CHCl_3$/*i*Pr_2O, →4 °C, −18 °C); $[\alpha]_D^{20}$ −50.59 (*c* 1.01, acetone). ^{1}H NMR (400.13 MHz, $CDCl_3$): δ 7.37 (d, J = 1.3 Hz, 1H), 7.18 (d, J = 1.3 Hz, 1H), 6.86 (d, J = 5.3 Hz, 1H), 5.82 (t, J = 5.3 Hz, 1H), 5.54 (dd, J = 5.3, 3.5 Hz, 1H), 5.18 (tdd, J = 13.0, 5.6, 3.7 Hz, 1H), 4.71 (dd, J = 5.6, 3.5 Hz, 1H), 4.63 (AB-part of ABX-system, J_{AB} = 10.4 Hz, $J_{AX} \approx J_{BX}$ = 3.7 Hz, 2H), 2.16 (s, 3H), 1.92 (s,3H), 1.85 (s, 3H). ^{13}C NMR (100.61 MHz, $CDCl_3$): δ 169.7, 168.9, 168.1, 144.5, 127.9, 122.4, 87.1, 81.8 (d, J = 4.6 Hz), 80.6 (d, J = 174.4 Hz), 70.9 (d, J = 19.1 Hz), 70.4 (2C), 20.8, 20.2, 19.7. IR (Si): ν 3016, 2970, 1743, 1366, 1228, 1217 cm^{-1}. Anal. Calcd for $C_{15}H_{18}FN_3O_9$ (403.32): C, 44.67; H, 4.50. Found: C, 44.56; H 4.31. The α-configuration at the anomeric carbon atom and the constitution of the compound was confirmed by X-ray structure analysis. For details, see Supporting information.

β-Anomer β-***11***: More polar than α-**11**, mp 77–78 °C (CH_2Cl_2/*i*Pr_2O), $[\alpha]_D^{20}$ +57.27 (*c* 1.03, acetone). ^{1}H NMR (400.13 MHz, $CDCl_3$): δ 7.30 (d, J = 1.1 Hz, 1H), 7.19 (d, J = 1.1 Hz, 1H), 6.61 (d, J = 4.4 Hz, 1H), 5.48 (dd, J = 5.7, 5.3 Hz, 1H), 5.41(dd, J = 5.7, 4.4 Hz, 1H), 5.30 (qd, J_{HF} = 22.2 Hz, J = 4.1 Hz, 1H), 4.60 (AB part of ABX system coupling with F, J_{HF} = 46.8 Hz, J_{AB} = 10.5 Hz, $J_{AX} = J_{BX}$ = 4.1 Hz, 2H), 4.44 (≈ t, J = 5.3 Hz, 1H), 2.13 (s, 3H), 2.10 (s, 3H), 2.09 (s, 3H). ^{13}C NMR (150.90 MHz, $CDCl_3$): δ 169.7, 169.2, 169.1, 144.4, 129.1, 121.0, 88.8, 80.5 (d, J = 175.0 Hz), 79.8 (d, J = 4.6 Hz), 74.5, 70.6 (J = 19.6 Hz), 69.3, 20.7, 20.3, 20.2. IR (ATR): ν 1761, 1746, 1350, 1240, 1219, 1098, 1079, 1061, 1017 cm^{-1}. Anal. Calcd for $C_{15}H_{18}N_3O_9$ (403.32): C, 44.67; H 4.50. Found: C, 44.66; H, 4.31.

4.5.6. 1-(6′-Deoxy-6′-fluoro-β-D-allofuranosyl)-2-nitroimidazole (β-1)

A solution of CH_3ONa in CH_3OH (0.1 mL, 1 M) was added to β-**11** (0.55 g, 1.36 mmol) dissolved in dry CH_3OH (4 mL) in a centrifuge

tube at 0 °C. After stirring for 1 h (after 5 min crystals started to form), small pieces of dry ice were added to neutralize the base. The crystals were collected by centrifugation (10 min, 3000 rpm), washed with CH_3OH (5 mL), again collected by centrifugation and dried (0.350 g, homogenous by ^1H NMR, contained 0.17 mol CH_3OH in crystals; it is possibly not necessary to crystallize from water). Crystallization from water (low solubility even in hot water) gave analytically pure 2-nitroimidazole nucleoside β-**1** (0.183 g, 61%) as colorless crystals; mp 189 °C (decomp.); $[\alpha]_D^{20}$ +8.68 (*c* 0.645, DMF). ^1H NMR (400.13 MHz, DMSO): δ 8.15 (s, 1H), 7.23 (s, 1H), 6.26 (d, J = 2.7 Hz, 1H), 5.85 (d, J = 5.1 Hz, 1H), 5.65 (d, J = 4.9 Hz, 1H), 5.15 (d, J = 5.9 Hz, 1H), 4.44 (ABX system, J_{HF} = 47.0 Hz, J_{AB} = 9.6 Hz, J_{AX} = 3.8 Hz, J_{BX} = 7.0 Hz, 2H), 4.21–4.08 (m, 3H, 2H), 3.97 (dd, J = 5.6, 3.8 Hz, 1H). ^{13}C NMR (100.61 MHz, DMSO): δ 144.5, 127.8, 123.4, 91.4, 84.1 (d, J = 167.3 Hz), 82.6 (d, J = 8.3 Hz), 75.9, 68.8 (d, J = 19.1 Hz), 67.9. IR (ATR): ν 3388, 3200, 3118, 1536, 1483, 1354, 1099, 988 cm^{-1}. Anal. Calcd for $C_9H_{12}FN_3O_6$ (277.21): C, 38.99; H, 4.36; N, 15.16. Found: C, 38.78; H, 4.16; N, 14.93.

4.6. Automated radiosynthesis of β-[^{18}F]1

Labeling reactions were performed using a TRACERLab FX N Pro automated synthesis module (GE Healthcare GmbH, Solingen, Germany). In the first step, cyclotron-produced [^{18}F]fluoride (140 ± 30 GBq) was trapped on a Chromafix-PS HCO_3^- anion exchange cartridge (Macherey–Nagel GmbH, Düren, Germany) preconditioned with EtOH (2 mL) and sterile H_2O (2.5 mL). Subsequently, the radioactivity was eluted with tetrabutylammonium hydrogen carbonate solution (58 mM, 0.5 mL) followed by CH_3CN (1 mL). Solvent was evaporated at 100 °C under a stream of argon followed by drying under vacuum. To the dried tetrabutylammonium [^{18}F]fluoride complex precursor β-**6** (7 mg, 14.4 μmol) dissolved in anhydrous DMSO (1 mL) was added followed by stirring at 115 °C for 8 min. After cooling to 40 °C, aqueous NaOH (0.25 M, 0.5 mL) was added followed by stirring for 1 min. For neutralization of the reaction mixture, H_3PO_4 (85% w/w, 0.25 mL) in DMSO (0.75 mL) was added. The reaction mixture was passed over a glass wool cartridge to remove insolubles and injected into the built-in semipreparative HPLC system. A Nucleosil 100-5C18 HD (290 × 8 mm) column (Macherey–Nagel GmbH, Düren, Germany) was eluted at a flow rate of 3 mL/min with 4% (v/v) EtOH in 50 mM NaH_2PO_4 solution. The HPLC eluate was monitored in series for radioactivity and ultraviolet (UV) absorption at a wavelength of 220 nm. On this system β-[^{18}F]**1** eluted with a retention time of 20–27 min. The collected product fraction was passed over a 0.22 μm sterile filter (Millex GV, Millipore, Bedford, MA, USA) and diluted with sterile saline solution to a final concentration of approximately 370 MBq/mL. Radiochemical and chemical purity as well as specific activity of β-[^{18}F]**1** was determined with analytical radio-HPLC using a Zorbax SB-Aq (5 μm, 250 × 4 mm) column (Agilent Technologies, Santa Clara, CA, USA) and a gradient of H_2O and CH_3CN as eluent (0–3 min: 5% CH_3CN, 3–7 min: 5–15% CH_3CN, 7–14 min: 15–85% CH_3CN, 14–19 min: 85% CH_3CN) at a flow rate 0.5 mL/min. The HPLC eluate was monitored in series for radioactivity (GABI*, raytest GmbH, Straubenhardt, Germany) and UV absorption (Agilent 1200, Agilent Technologies, Santa Clara, CA, USA) at a wavelength of 220 nm. On this system β-[^{18}F]**1** and β-**6** eluted with retention times of 7.8 and 15.6 min, respectively. Radio-TLC was performed on silica TLC plates (silica gel 60F 254 nm 20 × 20 cm, Merck, Darmstadt, Germany) using CH_3CN/H_2O (95/5, v/v) as mobile phase. Radioactivity distribution on developed plates was measured using a miniGITA system (raytest GmbH, Straubenhardt, Germany) showing an R_f-value of 0.65 for β-[^{18}F]**1**.

4.7. Inhibition of [^{3}H]uridine transport in *Saccharomyces cerevisiae*

Yeast (*S. cerevisiae*) were separately transformed with plasmids (pYPhENT1, pYPhENT2, pYPhCNT1, pYPhCNT2, or pYPhCNT3) encoding human nucleoside transporters (hNTs) (hENT1, hENT2, hCNT1, hCNT2, or hCNT3, respectively) as described elsewhere.[41,42] Uptake of 1 μM [^{3}H]uridine was measured as previously described using a semiautomated cell harvester (Micro96 HARVESTER, Skatron Instruments, Tranby, Norway).[22,43] Yeast cells were incubated with 1 μM [^{3}H]uridine in yeast growth media (pH 7.4) in the presence or absence (uninhibited controls) of graded concentrations (0–3 mM) of test compounds. Uridine self-inhibition was used to determine maximum inhibition of mediated transport. Concentration–effect curves were subjected to nonlinear regression analysis using Prism software (version 4.03; GraphPad Software Inc.) to obtain the concentration of test compound that inhibited uridine uptake by 50% relative to that of untreated cells (IC_{50} values). Each IC_{50} value determination was conducted with nine concentrations and four replicates per concentration and experiments were repeated two to three times.

4.8. Cell uptake assay

For cell uptake experiments 1 mL cell culture media containing 1×10^5 cells was seeded in 24-well plates (VWR, Leuven, Belgium) and pre-cultured in a humidified atmosphere for 48 h at 37 °C and 5% CO_2. After pre-culturing, the well plates were visually inspected for confluency and further incubated for 2 h in either hypoxic (1% O_2, 5% CO_2 in N_2) or normoxic (21% O_2, 5% CO_2 in air) atmosphere under otherwise identical conditions. In addition, 30 mL of the respective cell culture media was equilibrated for 2 h in either hypoxic or normoxic atmosphere. Subsequently, equilibrated cell culture media containing β-[^{18}F]**1** or [^{18}F]FDG (10 kBq/mL per well) was applied and plates were further incubated for 1, 3 or 5 h under hypoxic or normoxic atmosphere. Following incubation, medium was discarded and cells were washed twice with ice-cold PBS. Cells were detached by using 0.1 mL 0.25% (w/w) trypsin–EDTA solution and the cell suspension was transferred into test tubes. Radioactivity content in test tubes was measured using a gamma counter (Wizard 1470, Perkin Elmer, Wellesley, MA, USA). Each experiment was performed in quadruple and radiotracer uptake was expressed as mean decay corrected percent incubated dose per 10^5 seeded cells at start of the incubation period. Cell viability was assessed using water-soluble-tetrazolium (WST-1) assay according to manufacturer's instructions (see Supporting information).

4.9. Uptake inhibition assay

Cells (1×10^5 per well) were seeded in 24-well plates (VWR, Leuven, Belgium) and incubated for 48 h in either hypoxic (1% O_2, 5% CO_2 in N_2) or normoxic (21% O_2, 5% CO_2 in air) atmosphere. On the experimental day, growth media was aspirated, transport buffer containing 20 mM Tris, 3 mM K_2HPO_4 and 5 mM glucose with 144 mM NaCl, 1 mM $CaCl_2$ and 1.2 mM $MgCl_2$ was added and cells were further incubated for 1 h in the respective atmosphere. Afterwards transport buffer was removed from wells, buffer or buffer containing 10 μm of either dipyridamole or NBMPR was added and plates were pre-incubated for further 10 min followed by addition of β-[^{18}F]**1** and incubation for further 10 min. At the end of the uptake time, cells were washed with ice-cold buffer and solubilized using 1% Triton X-100. Solubilized cells were transferred into test tubes and radioactivity was measured using a gamma counter (Wizard 1470, Perkin Elmer, Wellesley, MA, USA). Each experiment was performed in quadruple and

radiotracer uptake was expressed as percent incubated dose per 10^5 cells.

4.10. Biodistribution studies in nude mice

Biodistribution of β-[^{18}F]**1** was assessed in anesthetized, female athymic nude NMRI-Foxn1^{nu} mice (n = 10), aged 10–12 weeks, weighing 28.1 ± 1.3 g which were assigned to two study groups. In group one, mice were anesthetized using isoflurane (2.5–3%) in air whereas in group two, procedures were performed using isoflurane (2.5–3%) in oxygen. Prior to intravenous injection, mice were placed on a heating pad (37 °C), pre-anesthetized for 30 min in their respective atmosphere and 7.1 ± 1.3 MBq β-[^{18}F]**1** in 0.1 mL was administered via a tail vein. After injection, animals were placed back on the heating pad and further kept under anesthesia for the whole uptake period in their respective atmosphere. Two hours after radiotracer administration, a terminal blood sample was withdrawn under anesthesia from the retrobulbar venous plexus and the animals were sacrificed by cervical dislocation. Blood was centrifuged to obtain plasma (17,000*g*, 4 °C, 4 min), tissues and urine were collected and samples were transferred into pre-weighted tubes. Radioactivity content in tissues was measured using a gamma counter (Wizard 1470, Perkin Elmer, Wellesley, MA, USA). The measured radioactivity data were corrected for radioactive decay and expressed as standardized uptake value (SUV = radioactivity per g/injected radioactivity × body weight).

4.11. Analysis of radiolabeled metabolites

Plasma samples were precipitated using methanol (2 μL per μL plasma), vortexed (3 min) and centrifuged (12,000*g*, rt, 5 min). Urine samples were diluted with methanol (50 μL per μL urine). Plasma supernatant, diluted urine and diluted radiotracer solution as reference (2 μL each) were spotted on a TLC plate (Merck silica gel 60F 254 nm, 20 × 20 cm) and plates were developed in CH_3CN/H_2O (95/5, v/v). Detection of radioactivity distribution was performed by placing the TLC plates on multi-sensitive phosphor screens (Perkin Elmer, Waltham, MA, USA) and subsequent scanning at 300 dpi resolution using a Phosphor imager (Cyclone Plus, Perkin Elmer, Waltham, MA, USA).

4.12. Small-animal PET imaging in EMT6 tumor bearing mice

Freshly harvested EMT6 cells (4×10^6), suspended in 0.1 mL sterile PBS were subcutaneously injected into the right shoulder region of female athymic nude NMRI-Foxn1^{nu} mice (n = 7), aged 10–12 weeks, weighing 26.3 ± 2.1 g. After approximately 10 d, when tumors reached a size of 980 ± 360 mm^3 and started to exhibit external signs of tumor necrosis, the imaging procedures were initiated. Imaging was performed in all animals (n = 4) on consecutive days as follows:

- Day 1: anatomical MRI and static [^{18}F]FDG PET;
- Day 2: dynamic β-[^{18}F]**1** PET under isoflurane/oxygen (100% O_2) 30 min prior injection and during the entire scan time;
- Day 3: dynamic β-[^{18}F]**1** PET under isoflurane/air (21% O_2) 30 min prior injection and during the entire scan time.

On day 1, mice were pre-anesthetized in an induction chamber using isoflurane (2.5–3.5% in oxygen) which was placed on a heating mat (38 °C). Subsequently, 5 ± 1 MBq [^{18}F]FDG in 0.1 mL sterile saline were injected intraperitoneally and animals were transferred to a heated animal bed (38 °C). Animal respiratory rate and body temperature were constantly monitored (SA Instruments Inc., Stony Brook, NY, USA) and the isoflurane level was adjusted (range: 1.5–2.5% in oxygen) to achieve a constant depth of anesthesia. Anatomical MRI was performed on a 1 T benchtop MRI (ICON, Bruker Biospin GmbH, Ettlingen, Germany) using a customized T_1-weighted gradient echo sequence (T1-FLASH) with the following imaging parameters: echo time (TE) = 4.7 ms; repetition time (TR) = 25 ms; flip angle (FA) = 25°; field of view (FOV) = 7.6 × 2.6 × 2.4 cm; matrix = 304 × 112; 32 slices; slice thickness = 750 μm; total imaging time = 15 min. Following MRI, the animal bed was transferred into the gantry of a microPET scanner (Focus 220, Siemens Medical Solutions, Knoxville, TN, USA) and a 10 min transmission scan using a rotating ^{57}Co point source was recorded. At 60 min after [^{18}F]FDG injection, a 15 min static PET scan (energy window = 250–750 keV; timing window = 6 ns) was acquired.

On day 2, mice were pre-anesthetized in an induction chamber using isoflurane (2.5–3.5% in oxygen), positioned on a heated animal bed (m2m imaging Corp, Cleveland, OH, USA) and the lateral tail veins were cannulated. Two mice were imaged simultaneously in one PET image acquisition. Animal monitoring and adjustment of depth of anesthesia were performed like described above. The animal bed was positioned in the center of the microPET scanner and a 10 min transmission scan was recorded. Subsequently, 30 min after induction of anesthesia, 0.1 mL β-[^{18}F]**1** (6.4 ± 0.4 MBq) was injected as an intravenous bolus over 60 s and a 2 h dynamic PET scan (energy window = 250–750 keV; timing window = 6 ns) was initiated at start of radiotracer injection. At the end of PET data acquisition, a blood sample was withdrawn under isoflurane anesthesia from the retrobulbar venous plexus. Blood was centrifuged to obtain plasma, (17,000*g*, 4 °C, 4 min) and aliquots of blood and plasma were transferred into pre-weighted test tubes. Radioactivity content was measured in a gamma counter. The measured radioactivity data were corrected for radioactive decay and expressed as SUV.

On day 3 dynamic PET imaging was repeated as described on day 2 with the exception that all anesthesia was performed using isoflurane in medical air (21% O_2) and the injected β-[^{18}F]**1** activity was 7.2 ± 0.9 MBq.

Dynamic PET emission data was sorted into 24 frames, which incrementally increased in time length from 5 s to 20 min. All PET images were reconstructed using Fourier rebinning of the 3D sinograms followed by two-dimensional filtered back projection with a ramp filter, resulting in a voxel size of 0.4 × 0.4 × 0.798 mm^3. The standard data correction protocol (normalization, attenuation and decay correction) was applied to the PET data. The PET units were converted into units of radioactivity by applying a calibration factor derived from imaging of a cylindrical phantom (volume ~ 70 cm^3) with a known ^{18}F-radioactivity concentration. Using the image analysis software AMIDE[44], volumes of interest (VOI) were manually drawn covering the whole tumor area on the reconstructed PET images. An elliptical reference VOI was placed on the left subscapular muscle as reference region. For quantitation of radioactivity uptake in tissues only voxels exhibiting >75% of the maximum radioactivity uptake were used and expressed as standardized uptake value for the maximum 25 percent of voxels (SUV_{max25}). Tumor-to-muscle ratios were calculated by dividing the radioactive uptake in tumor tissue by the corresponding radioactivity calculated for the reference region. Tumor-to-blood ratios were calculated by dividing the tumor radioactivity concentration in the last PET frame (100–120 min) by the corresponding blood radioactivity concentration as determined by the gamma counter measurements after the PET scan (~123 min).

4.13. Autoradiography

EMT6 tumor bearing mice (n = 3) were anesthetized using isoflurane in air (2.0–2.5%), placed on a heating mat (38 °C) and

the tail veins were cannulated. After 25 min, pimonidazole hydrochloride in saline (60 mg/kg, 0.05 mL) was injected intravenously and the catheters were flushed with sterile saline solution (0.05 mL). After additional 5 min, 0.1 mL β-[^{18}F]**1** (15.0 ± 2.3 MBq) was injected as bolus over 60 s, the animals were placed back on the heating mat and anesthesia was maintained for further 2 h using isoflurane/air (1.5–2.0%). Monitoring of breathing rate and body temperature as well as adjustment of depth of anesthesia was performed as described in the previous section. After the uptake period, animals were sacrificed by cervical dislocation while still under anesthesia. Tumors were immediately excised, embedded in freezing medium (Tissue-Tek, Sakura, The Netherlands) and snap-frozen in isopentane cooled in liquid nitrogen. Subsequently, tumors were cut into 10 μm slices using a cryostat (Microm HM 550, Walldorf, Germany) at −14 °C and consecutive tumor sections were mounted on SuperFrost Plus slides (Menzel, Braunschweig, Germany). Immediately after cutting, a set of tumor sections was placed into film cassettes and exposed overnight to multisensitive phosphor screens (Perkin Elmer, Waltham, MA, USA). The remainder of the slides was used for immunohistochemistry and histologic staining. The exposed phosphor screens were removed from the film cassettes under dim light conditions and scanned at 600 dpi resolution using a Phosphor imager (Cyclone Plus, Perkin Elmer, Waltham, MA, USA). Images were analyzed using the systems Optiquant v5.0 software.

4.14. Pimonidazole immunohistochemistry and histologic staining

For immunohistochemical detection of hypoxia, EMT6 tumor slides were fixed in cold acetone (4 °C) for 10 min, washed in PBS containing 0.2% (v/v) Tween 20 (PBST) and endogenous peroxidase activity was quenched by incubation with 0.4% (v/v) hydrogen peroxide in PBST. After blocking, sections were incubated at 4 °C overnight with rabbit anti-pimonidazole antibody diluted 1:50 in antibody diluent. Subsequently, slides were rinsed with cold PBS and then incubated for 90 min with biotinylated donkey anti-rabbit antibody (1:500 in antibody diluent). Staining was intensified using avidin–biotin–peroxidase complex and visualized by diaminobenzidine (DAB) reaction in the presence of 0.01% (v/v) hydrogen peroxide. The washed and dehydrated slides were coverslipped with Entellan. As negative control the primary antibody was replaced by antibody diluent which resulted in negative staining. Slides were digitized using a digital brightfield slide scanner (Pannoramic DESK, 3dhistech, Budapest, Hungary) and processing of imaging data was performed using the built-in Pannoramic Viewer software (v1.15).

For hematoxylin and eosin (H&E) staining, consecutive slides were fixed in cold acetone (4 °C) for 10 min and further processed according to standard laboratory procedures.[45]

Author contributions

The manuscript was written through contributions of all authors. All authors have given approval to the final version of the manuscript.

Funding sources

The research leading to these results has received funding from the Lower Austria corporation for research and education (NFB) under grant agreement number LS11-002 awarded to C. Kuntner.

Acknowledgments

The authors thank the radiochemistry staff (Seibersdorf labor GmbH) for their skillful assistance, Andreas Eger (IMC University of Applied Science Krems) for helpful advice regarding cell culture and viability assays, Susanne Felsinger for recording NMR spectra and Johannes Theiner for combustion analysis.

A. Supplementary data

Supplementary data (^{1}H and ^{13}C NMR spectra of synthesized compounds. X-ray structure analysis of α-**11**. HPLC and radio-TLC chromatograms of β-[^{18}F]**1**. Cell viability assessment and in vitro cell uptake of [^{18}F]FDG) associated with this article can be found, in the online version, at http://dx.doi.org/10.1016/j.bmc.2016.08.053.

References and notes

1. Chapman, J. D. *Cancer* **1984**, *54*, 2441.
2. Hockel, M.; Schlenger, K.; Knoop, C.; Vaupel, P. *Cancer Res.* **1991**, *51*, 6098.
3. Vaupel, P.; Schlenger, K.; Knoop, C.; Hockel, M. *Cancer Res.* **1991**, *51*, 3316.
4. Brown, J. M. *Cancer Res.* **1999**, *59*, 5863.
5. Nunn, A.; Linder, K.; Strauss, H. W. *Eur. J. Nucl. Med.* **1995**, *22*, 265.
6. Kumar, P.; Bacchu, V.; Wiebe, L. I. *Sem. Nucl. Med.* **2015**, *45*, 122.
7. Mees, G.; Dierckx, R.; Vangestel, C.; Van de Wiele, C. *Eur. J. Nucl. Med. Mol. Imaging* **2009**, *36*, 1674.
8. Masaki, Y.; Shimizu, Y.; Yoshioka, T.; Tanaka, Y.; Nishijima, K.; Zhao, S.; Higashino, K.; Sakamoto, S.; Numata, Y.; Yamaguchi, Y.; Tamaki, N.; Kuge, Y. *Sci. Rep.* **2015**, *5*, 16802.
9. Hendrickson, K.; Phillips, M.; Smith, W.; Peterson, L.; Krohn, K.; Rajendran, J. *Radiother. Oncol.* **2011**, *101*, 369.
10. Lin, Z.; Mechalakos, J.; Nehmeh, S.; Schoder, H.; Lee, N.; Humm, J.; Ling, C. C. *Int. J. Radiat. Oncol. Biol. Phys.* **2008**, *70*, 1219.
11. Mortensen, L. S.; Buus, S.; Nordsmark, M.; Bentzen, L.; Munk, O. L.; Keiding, S.; Overgaard, J. *Acta Oncol.* **2010**, *49*, 934.
12. Rasey, J. S.; Koh, W. J.; Evans, M. L.; Peterson, L. M.; Lewellen, T. K.; Graham, M. M.; Krohn, K. A. *Int. J. Radiat. Oncol. Biol. Phys.* **1996**, *36*, 417.
13. Thorwarth, D.; Eschmann, S. M.; Holzner, F.; Paulsen, F.; Alber, M. *Radiother. Oncol.* **2006**, *80*, 151.
14. Rasey, J. S.; Hofstrand, P. D.; Chin, L. K.; Tewson, T. J. *J. Nucl. Med.* **1999**, *40*, 1072.
15. Fleming, I. N.; Manavaki, R.; Blower, P. J.; West, C.; Williams, K. J.; Harris, A. L.; Domarkas, J.; Lord, S.; Baldry, C.; Gilbert, F. J. *Br. J. Cancer* **2015**, *112*, 238.
16. Piert, M.; Machulla, H. J.; Picchio, M.; Reischl, G.; Ziegler, S.; Kumar, P.; Wester, H. J.; Beck, R.; McEwan, A. J. B.; Wiebe, L. I.; Schwaiger, M. *J. Nucl. Med.* **2005**, *46*, 106.
17. Postema, E. J.; McEwan, A. J.; Riauka, T. A.; Kumar, P.; Richmond, D. A.; Abrams, D. N.; Wiebe, L. I. *Eur. J. Nucl. Med. Mol. Imaging* **2009**, *36*, 1565.
18. Reischl, G.; Ehrlichmann, W.; Bieg, C.; Solbach, C.; Kumar, P.; Wiebe, L. I.; Machulla, H. J. *Appl. Radiat. Isot.* **2005**, *62*, 897.
19. Sorger, D.; Patt, M.; Kumar, P.; Wiebe, L. I.; Barthel, H.; Seese, A.; Dannenberg, C.; Tannapfel, A.; Kluge, R.; Sabri, O. *Nucl. Med. Biol.* **2003**, *30*, 317.
20. Reischl, G.; Dorow, D. S.; Cullinane, C.; Katsifis, A.; Roselt, P.; Binns, D.; Hicks, R. J. *J. Pharm. Pharm. Sci.* **2007**, *10*, 203.
21. Patt, M.; Sorger, D.; Scheunemann, M.; Stocklin, G. *Appl. Radiat. Isot.* **2002**, *57*, 705.
22. Emami, S.; Kumar, P.; Yang, J.; Kresolic, Z.; Paproski, R.; Cass, C.; McEwan, A. J. B.; Wiebe, L. I. *J. Pharm. Pharm. Sci.* **2007**, *10*, 237.
23. Kumar, P.; Emami, S.; Kresolek, Z.; Yang, J.; McEwan, A. J. B.; Wiebe, L. I. *Med. Chem.* **2009**, *5*, 118.
24. Young, J. D.; Yao, S. Y.; Baldwin, J. M.; Cass, C. E.; Baldwin, S. A. *Mol. Aspects Med.* **2013**, *34*, 529.
25. Zsoldos-Mády, V.; Zbiral, E. *Monatsh. Chem.* **1986**, *117*, 1325.
26. Schweifer, A.; Hammerschmidt, F. *J. Org. Chem.* **2011**, *76*, 8159.
27. Schulze, O.; Voss, J.; Adiwidjaja, G. *Carbohydr. Res.* **2005**, *340*, 587.
28. Akiyama, Y.; Hiramatsu, C.; Fukuhara, T.; Hara, S. *J. Fluorine Chem.* **2006**, *127*, 920.
29. Burgman, P.; O'Donoghue, J. A.; Humm, J. L.; Ling, C. C. *J. Nucl. Med.* **2001**, *42*, 170.
30. Damaraju, V. L.; Scriver, T.; Mowles, D.; Kuzma, M.; Ryan, A. J.; Cass, C. E.; Sawyer, M. B. *Clin. Cancer Res.* **2014**, *20*, 176.
31. Hoigebazar, L.; Jeong, J. M.; Lee, J. Y.; Shetty, D.; Yang, B. Y.; Lee, Y. S.; Lee, D. S.; Chung, J. K.; Lee, M. C. *J. Med. Chem.* **2012**, *55*, 3155.
32. Bonnitcha, P. D.; Vavere, A. L.; Lewis, J. S.; Dilworth, J. R. *J. Med. Chem.* **2008**, *51*, 2985.
33. Maier, F. C.; Kneilling, M.; Reischl, G.; Cay, F.; Bukala, D.; Schmid, A.; Judenhofer, M. S.; Rocken, M.; Machulla, H. J.; Pichler, B. J. *Radiat. Oncol.* **2011**, *6*, 165.

34. Mahling, M.; Fuchs, K.; Thaiss, W. M.; Maier, F. C.; Feger, M.; Bukala, D.; Harant, M.; Eichner, M.; Reutershan, J.; Lang, F.; Reischl, G.; Pichler, B. J.; Kneilling, M. *PLoS One* **2015**, *10*, e0124665.
35. Piert, M.; Machulla, H. J.; Picchio, M.; Reischl, G.; Ziegler, S.; Kumar, P.; Wester, H. J.; Beck, R.; McEwan, A. J.; Wiebe, L. I.; Schwaiger, M. *J. Nucl. Med.* **2005**, *46*, 106.
36. Engelhardt, E. L.; Schneider, R. F.; Seeholzer, S. H.; Stobbe, C. C.; Chapman, J. D. *J. Nucl. Med.* **2002**, *43*, 837.
37. Moulder, J. E.; Rockwell, S. *Int. J. Radiat. Oncol. Biol. Phys.* **1984**, *10*, 695.
38. Carreau, A.; El Hafny-Rahbi, B.; Matejuk, A.; Grillon, C.; Kieda, C. *J. Cell. Mol. Med.* **2011**, *15*, 1239.
39. Dubois, L.; Landuyt, W.; Haustermans, K.; Dupont, P.; Bormans, G.; Vermaelen, P.; Flamen, P.; Verbeken, E.; Mortelmans, L. *Br. J. Cancer* **2004**, *91*, 1947.
40. Haga, M.; Takano, M.; Tejima, S. *Carbohydr. Res.* **1972**, *21*, 440.
41. Vickers, M. F.; Kumar, R.; Visser, F.; Zhang, J.; Charania, J.; Raborn, R. T.; Baldwin, S. A.; Young, J. D.; Cass, C. E. *Biochem. Cell Biol.* **2002**, *80*, 639.
42. Zhang, J.; Visser, F.; Vickers, M. F.; Lang, T.; Robins, M. J.; Nielsen, L. P.; Nowak, I.; Baldwin, S. A.; Young, J. D.; Cass, C. E. *Mol. Pharmacol.* **2003**, *64*, 1512.
43. Vickers, M. F.; Zhang, J.; Visser, F.; Tackaberry, T.; Robins, M. J.; Nielsen, L. P.; Nowak, I.; Baldwin, S. A.; Young, J. D.; Cass, C. E. *Nucleos. Nucleot. Nucl. Acids* **2004**, *23*, 361.
44. Loening, A. M.; Gambhir, S. S. *Mol. Imaging* **2003**, *2*, 131.
45. Cardiff, R. D.; Miller, C. H.; Munn, R. J. *Cold Spring Harb. Protoc.* **2014**, *2014*, 655.

Please cite this article in press as: Wanek, T.; et al. *Bioorg. Med. Chem.* (2016), http://dx.doi.org/10.1016/j.bmc.2016.08.053